iScience

CellPress

Article

Nuclear Actin Polymerized by mDia2 Confines Centromere Movement during CENP-A Loading

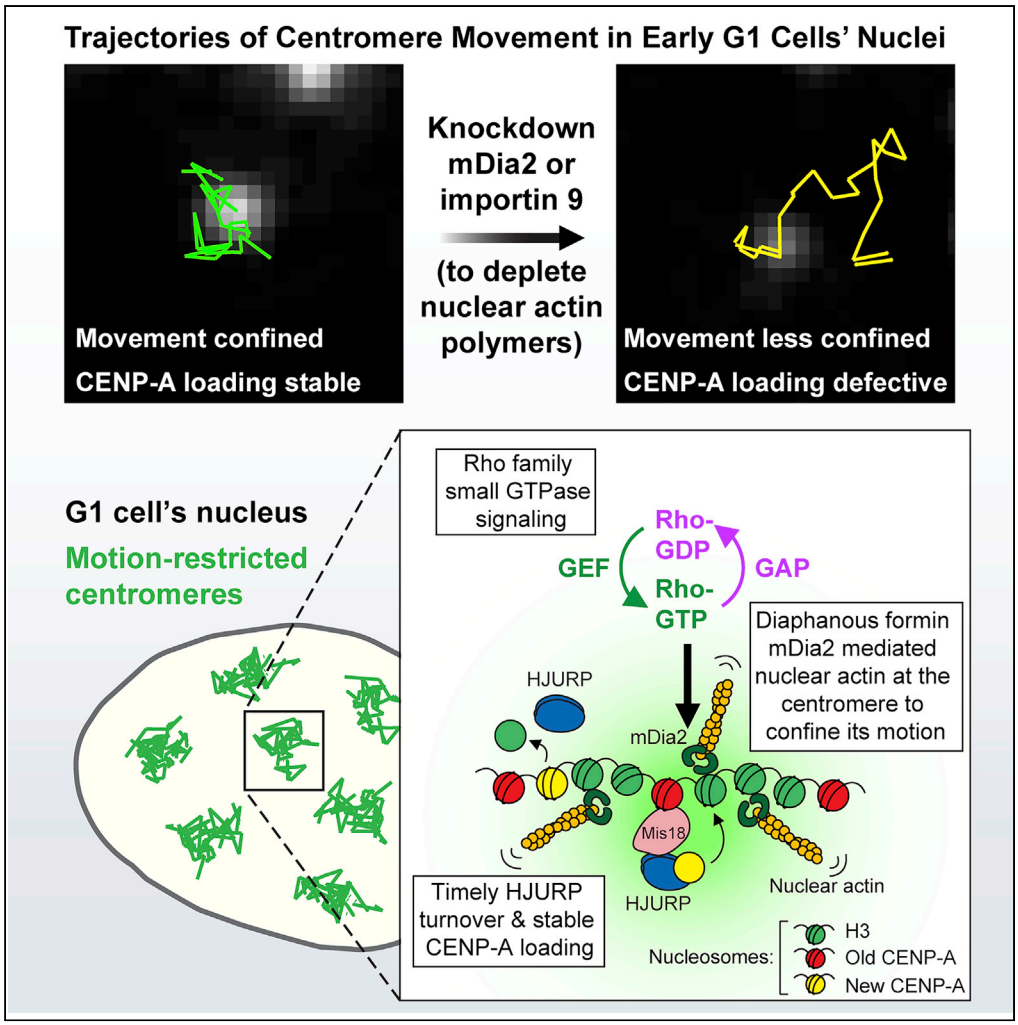

Chenshu Liu,
Ruijun Zhu,
Yinghui Mao

chenshu.liu@berkeley.edu (C.L.)
ym2183@cumc.columbia.edu (Y.M.)

HIGHLIGHTS

Formin mDia2 is required for nuclear actin polymerization at G1 centromeres

Nuclear actin polymerization is required to maintain centromeric CENP-A levels

mDia2 and nuclear actin restrict centromere movement during CENP-A loading

Nuclear actin and MgcRacGAP are required for timely turnover of centromeric HJURP

Liu et al., iScience 9, 314–327
November 30, 2018
https://doi.org/10.1016/j.isci.2018.10.031

iScience

CellPress

Article

Nuclear Actin Polymerized by mDia2 Confines Centromere Movement during CENP-A Loading

Chenshu Liu,[1,2,4,5,*] Ruijun Zhu,[1,3,4] and Yinghui Mao[1,*]

SUMMARY

Centromeres are specialized chromosomal regions epigenetically defined by the histone H3 variant centromere protein A (CENP-A). CENP-A needs to be replenished in every cell cycle, but how new CENP-A is stably incorporated into centromeric chromatin remains unclear. We have discovered that a cytoskeletal protein, diaphanous formin mDia2, is essential for the stable incorporation of new CENP-A proteins into centromeric nucleosomes. Here we report that mDia2-mediated formation of dynamic and short nuclear actin filaments in G1 nucleus is required to maintain CENP-A levels at the centromere. Importantly, mDia2 and nuclear actin are required for constrained centromere movement during CENP-A loading, and depleting nuclear actin or MgcRacGAP, which lies upstream of mDia2, extends centromeric association of the CENP-A loading chaperone Holliday junction recognition protein (HJURP). Our findings thus suggest that nuclear actin polymerized by mDia2 contributes to the physical confinement of G1 centromeres so that HJURP-mediated CENP-A loading reactions can be productive, and centromere's epigenetic identity can be stably maintained.

INTRODUCTION

Accurate segregation of chromosomes during mitosis relies on the existence and integrity of centromeres, chromosomal regions that are epigenetically determined by nucleosomes containing the histone H3 variant centromere protein A (CENP-A) (Cleveland et al., 2003). After the genome replicates in S phase, all CENP-A molecules redistribute to two sister chromatids, thus the total number of CENP-A molecules per centromere is reduced by half. It is therefore necessary to replenish the amount of CENP-A molecules at each centromere in every cell cycle, to ensure the stable inheritance of centromere identity over many generations of cell divisions. In mammals, new CENP-A proteins synthesized in the previous cell cycle are loaded at each centromere during the early G1 phase of the next cell cycle (Jansen et al., 2007). Many factors have been identified to be responsible for the initiation and execution of recruiting newly synthesized CENP-A molecules to the centromeres (Dunleavy et al., 2009; Foltz et al., 2009; Fujita et al., 2007; Maddox et al., 2007; McKinley and Cheeseman, 2014; Moree et al., 2011; Silva et al., 2012); among them is the Holliday junction recognition protein (HJURP) that functions as a chaperone to assemble new CENP-A molecules into nucleosomes (Barnhart et al., 2011). However, it remains unclear how new CENP-A molecules become stably incorporated into centromeric nucleosomes.

The male germ cell Rac GTPase-activating protein (MgcRacGAP), as well the small Rho GTPases under its regulation, Cdc42 and Rac1, have been shown to be essential for stabilizing newly loaded CENP-A at centromeres (Lagana et al., 2010). The diaphanous formin (mDia) proteins are important small Rho GTPase effectors and can regulate cytoskeletal dynamics by stabilizing microtubules and nucleating filamentous actin in a linear fashion (Chesarone et al., 2010). Previously we have reported that formin mDia2 is required for maintaining CENP-A levels at the centromere (Liu and Mao, 2016, Liu and Mao, 2017). Importantly, overexpressing a constitutively active form of mDia2 can rescue defective centromeric CENP-A levels caused by depleting MgcRacGAP. Nevertheless, the mechanisms by which mDia2 functions to promote stable CENP-A loading remains elusive. Among all three members of the mammalian diaphanous formin family, only mDia2, but not mDia1 or 3, can redistribute extensively from the cytoplasm to the nucleus and can biochemically associate with a number of nuclear proteins including histones and topoisomerases via its formin homology (FH) 2 domain (Daou et al., 2014; Miki et al., 2009). Inside the nucleus, mDia2 can effectively nucleate filamentous actin polymers (Baarlink et al., 2013). Accumulating evidence demonstrates that filamentous actin polymerized inside the nucleus plays important

[1]Department of Pathology and Cell Biology, Columbia University Vagelos College of Physicians and Surgeons, 630 W 168th Street, New York, NY 10032, USA

[2]Present address: Department of Molecular and Cell Biology, University of California, Berkeley, Berkeley, CA 94720, USA

[3]Present address: Department of Physiology, University of California, San Francisco, San Francisco, CA 94158, USA

[4]These authors contributed equally

[5]Lead Contact

*Correspondence: chenshu.liu@berkeley.edu (C.L.), ym2183@cumc.columbia.edu (Y.M.)

https://doi.org/10.1016/j.isci.2018.10.031

roles in regulating chromosome dynamics, including repositioning of chromosomal loci (Dundr et al., 2007), initiation of DNA replication (Parisis et al., 2017), response to and repair of DNA double-strand breaks (DSBs) (Belin et al., 2015; Wang et al., 2017), interactions with chromatin remodeling complexes (Andrin and Hendzel, 2004; Rando et al., 2002), and cross talk with important epigenetic enzymes (Serebryannyy et al., 2016). Of particular interest is the recent observation of filamentous nuclear actin with chromobodies right after mitotic exit during nuclear volume expansion and chromatin decondensation (Baarlink et al., 2017), which shares a similar time window of CENP-A loading in early G1. It is therefore intriguing to ask whether nuclear actin polymerized by mDia2 directly contributes to the stable loading of CENP-A at G1 centromeres.

Using a utrophin-based probe that visualizes polymeric nuclear actin, here we provide direct evidence that mDia2 is required for polymerizing nuclear actin in G1 and that polymerization-competent nuclear actin is required for maintaining CENP-A levels at the centromere. Importantly, both mDia2 and nuclear actin are required to restrict centromere movement during CENP-A loading, and the absence of nuclear actin or MgcRacGAP results in prolonged centromere association of HJURP, the molecular chaperone that transiently localizes to the centromere to assemble new CENP-A nucleosomes.

RESULTS

Formin mDia2 Is Required for the Formation of Short and Dynamic Nuclear Actin Filaments Visualized by the Utr230-EGFP-NLS Probe in G1 Phase

We have shown that the formin mDia2 and its nuclear localization are required to maintain CENP-A levels at centromeres (Liu and Mao, 2016). However, whether this novel role for mDia2 requires mDia2-mediated nuclear actin polymerization remains unresolved. Although latrunculin A or cytochalasin D treatment does not affect CENP-A levels at centromeres (Lagana et al., 2010), actin in the nucleus can form short oligomers or other forms of structures that are less sensitive to drug treatment (Belin et al., 2013; Gonsior et al., 1999; McDonald et al., 2006; Schoenenberger et al., 2005). To examine if there are actin filaments inside the nucleus concurrent with CENP-A loading, a utrophin-based nuclear actin probe, Utr230-EGFP-NLS (nuclear localization signal) (Belin et al., 2013; Table S1), was transiently expressed in synchronized HeLa cells transfected with mDia2 or GAPDH (control) small interfering RNA (Figure 1A; Table S2). Short-term live cell imaging revealed that about 40% of control G1 cells showed dynamic and short nuclear actin filaments with a typical "nuclear puncta" pattern. In contrast, the percentage of cells with nuclear puncta pattern was significantly reduced upon mDia2 depletion (Figures 1B and 1C; Video S1). Longer term live cell imaging from mitotic exit all the way into G1 was also carried out with cells stably expressing Utr230-EGFP-NLS. Apparent nuclear punctate signals of Utr230-EGFP-NLS were observed after cells enter G1 (approximately 46 min after anaphase onset on average), and once they appeared the punctate signals inside the nucleus remain visible for 176 min on average, although individual punctum did not necessarily persist throughout the whole time (Figures 1D, 1E, and S1; Videos S2 and S3). However, the occurrence and duration of nuclear punctate Utr230-EGFP-NLS were significantly reduced upon mDia2 depletion (Figures 1D, 1E, and S1; Video S2). To further examine at higher resolution the localization of these nuclear puncta in relation to centromeres, synchronized early G1 cells stably expressing Utr230-EGFP-NLS were fixed and stained for centromere marker (ACA). Remarkably, nuclear actin polymers visualized by the Utr230-EGFP-NLS probe, although exhibit punctate morphology throughout the nucleoplasm, have apparent enrichment in the vicinity of some but not all centromeres in the nucleus (Figure 1F; Video S4), and both the intensity enrichment of Utr230-EGFP-NLS adjacent to centromeres and the percentage of centromeres with adjacent Utr230-EGFP-NLS puncta per nucleus were significantly reduced upon mDia2 depletion (Figures 1F–1H). These results support the existence of short and dynamic nuclear actin polymers in early G1 cells concurrent with CENP-A loading, dependent on mDia2.

To examine whether actin polymerization activity is required for mDia2 function in stable CENP-A assembly we used quantitative imaging and the integrated nuclear CENP-A (INCA) algorithm that we developed for automated measurement (Liu and Mao, 2016). K853A mutation was introduced to the FH2 domain of full-length mDia2, as this mutant is known to be defective in actin polymerization (Bartolini et al., 2008). Similar to the actin mutations in the constitutively active mDia2-FH1FH2 fragment (Bartolini et al., 2008; Liu and Mao, 2016), K853A mutation in full-length mDia2 failed to restore the decreased CENP-A levels at centromeres upon depleting endogenous mDia2 (Figures S2A and S2B). This further supports that the actin nucleation activity of mDia2 is important for its role in CENP-A loading.

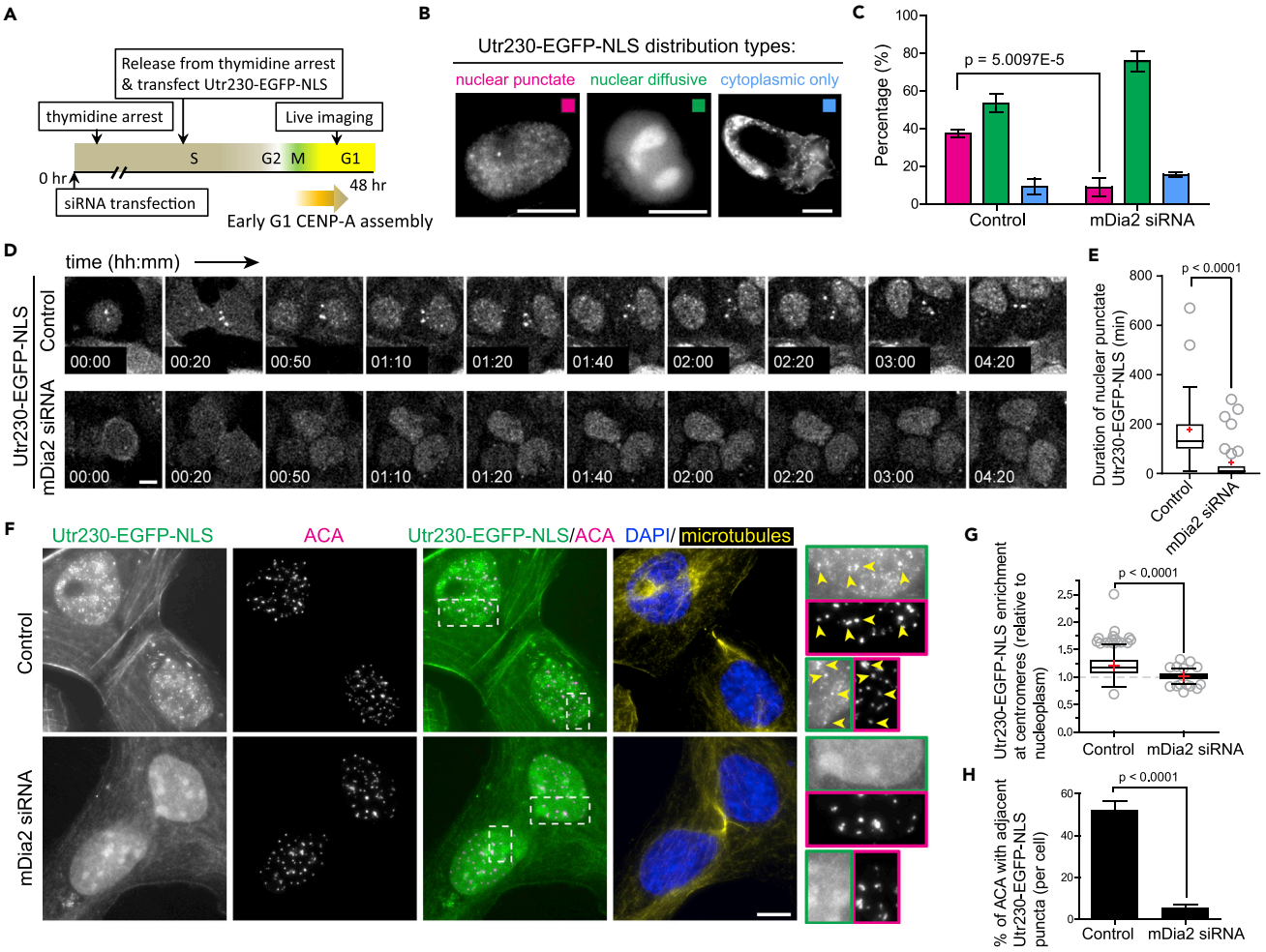

Figure 1. Formin mDia2 Is Required for the Utr230-EGFP-NLS Visualized Nuclear Actin Polymerization in the Vicinity of G1 Cells' Centromeres

(A) Schematics for transfection of mDia2 small interfering RNA (siRNA) (co-transfected with marker mCherry), as well as subsequent transient transfection of the nuclear actin probe Utr230-EGFP-NLS.

(B) Three distinctive distribution categories of Utr230-EGFP-NLS observed in G1 cells 12 hr after release from thymidine arrest. "Nuclear diffusive" is characterized by the lack of any apparent puncta inside the nucleus. See Methods for details. Scale bar, 10 μm. See also Video S1.

(C) The percentage of cells exhibiting each type of Utr230-EGFP-NLS distribution after being transfected with control (GAPDH) or mDia2 siRNA (n > 50 cells pooled from three independent transfections). Error bars show standard deviations of three experiments. The p value was computed using two-tailed z-test comparing two-sample proportions.

(D) Live imaging frames showing cells stably expressing Utr230-EGFP-NLS from mitotic exit to G1, with control or mDia2 siRNA transfection. The last frame before anaphase onset was aligned to be time point 00:00 (hr:min). Images were identically scaled over time for both control and mDia2 knockdown. Apparent cytoplasmic aggregates sometimes already exist even in mitosis. Scale bar, 10 μm. See also Videos S2 and S3.

(E) Whisker-Tukey boxplots quantifying the duration of the appearance of nuclear punctate Utr230-EGFP-NLS per cell. The center bars denote the median, and the + marks denote the mean. The p value was computed using two-tailed t test. Total measurement of 31 control cells and 31 mDia2 knockdown cells. See also Figure S1.

(F) Representative immunofluorescence images showing colocalization between nuclear Utr230-EGFP-NLS puncta and ACA (centromere marker) in G1 cells, with control or mDia2 siRNA transfection. Scale bar, 10 μm. Insets are 2× magnified with color-coded border for either Utr230-EGFP-NLS (green) or ACA (magenta). See also Video S4.

(G) Whisker-Tukey boxplots showing the enrichment of Utr230-EGFP-NLS in the vicinity of centromeres by quantifying the ratio of the intensity of Utr230-EGFP-NLS at all centromeres in a given nucleus over the nucleoplasmic intensity of Utr230-EGFP-NLS (excluded from centromeres). Each data point is the measurement for one centromere. The center bars denote the median, and the + marks denote the mean. The p value was computed using two-tailed t test. Total measurement of 736 centromeres from 13 control cells and 525 centromeres from 11 mDia2 knockdown cells.

(H) Mean percentages of centromeres with adjacent Utr230-EGFP-NLS puncta per cell. Error bars show SEM. The p value was computed using a two-tailed Mann-Whitney test. Total measurement of 18 control cells and 16 mDia2 knockdown cells.

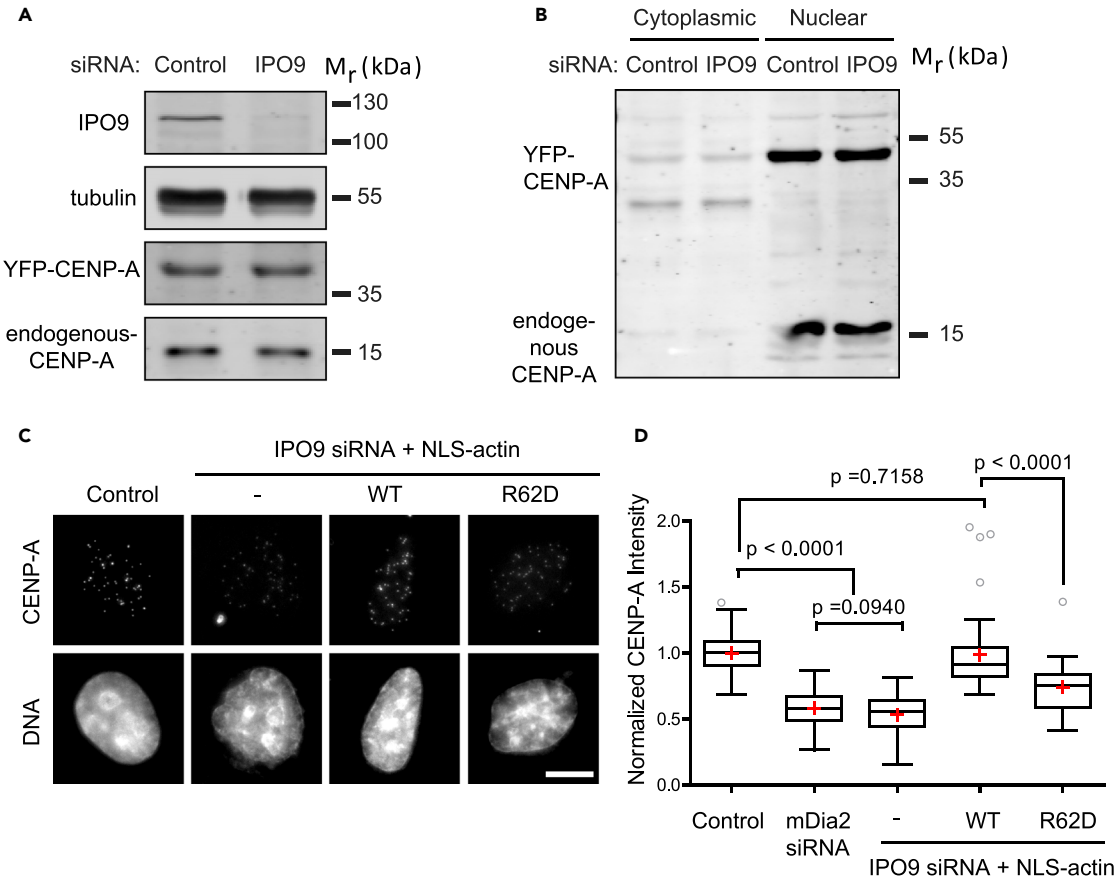

Figure 2. Nuclear Actin Polymerization Is Important for Maintaining CENP-A Levels at the Centromeres

(A and B) Depleting IPO9 does not change the levels of CENP-A inside the nucleus. (A) Total YFP-CENP-A and endogenous CENP-A were immunoblotted for control and IPO9 knockdown. (B) CENP-A levels were immunoblotted using cell lysates separated into cytoplasmic and nuclear fractions in both control and IPO9 knockdown.

(C) Polymerizable actin inside the nucleus rescues reduced CENP-A levels caused by IPO9 knockdown. Representative immunofluorescence images showing CENP-A levels at centromeres. DNA are stained with DAPI. Scale bar, 10 μm.

(D) Quantification of the normalized CENP-A integrated intensity per nucleus demonstrated by Whisker-Tukey boxplots. The center bars denote the median, and the + marks denote the mean. The p values were computed using two-tailed t test. Total measurement of 74 (control), 42 (mDia2 small interfering RNA [siRNA]), 50 (IPO9 siRNA), 52 (IPO9 siRNA + NLS-actin-WT), and 35 (IPO9 siRNA + NLS-actin-R62D) cells. See also Figure S2.

Actin Polymerization Inside the Nucleus Is Important for Stable Maintenance of CENP-A Levels at the Centromeres

To test the hypothesis that filamentous nuclear actin polymerized by mDia2 directly participates in stable CENP-A incorporation at the centromere, we set out altering the pool of actin inside the nucleus. Importin 9 (IPO9) has been shown to be responsible for shuttling actin monomers into the nucleus (Dopie et al., 2012). Knocking down IPO9 depletes the pool of actin proteins inside the nucleus, but neither does it change the total amount of YFP-CENP-A or untagged CENP-A proteins nor does it alter the relative distribution of CENP-A proteins in the cytoplasm or nucleus upon cellular fractionation (Figures 2A, 2B, and S2C). To evaluate only the "loading" machineries of CENP-A at centromeres, we expressed NLS-tagged actin constructs that accumulate in the nucleus independent of IPO9 (Belin et al., 2015) (Figure S2D). Like nuclear actin polymers visualized by Utr230-EGFP-NLS, wild-type NLS-FLAG-actin shows short punctate filaments inside the nucleus, whereas the polymerization-incompetent R62D mutant remains mostly diffusive in cells depleted of IPO9 (Figure S2D). IPO9 depletion resulted in a CENP-A loading phenotype comparable to that caused by mDia2 depletion. Significantly, the wild-type polymerizable actin tagged with NLS can effectively restore the reduced CENP-A levels upon IPO9 depletion, whereas the nonpolymerizable (Posern et al., 2002) R62D mutant of actin cannot (Figures 2C and 2D). These results collectively suggest that actin polymerization inside the nucleus is essential for the stable maintenance of CENP-A levels at centromeres.

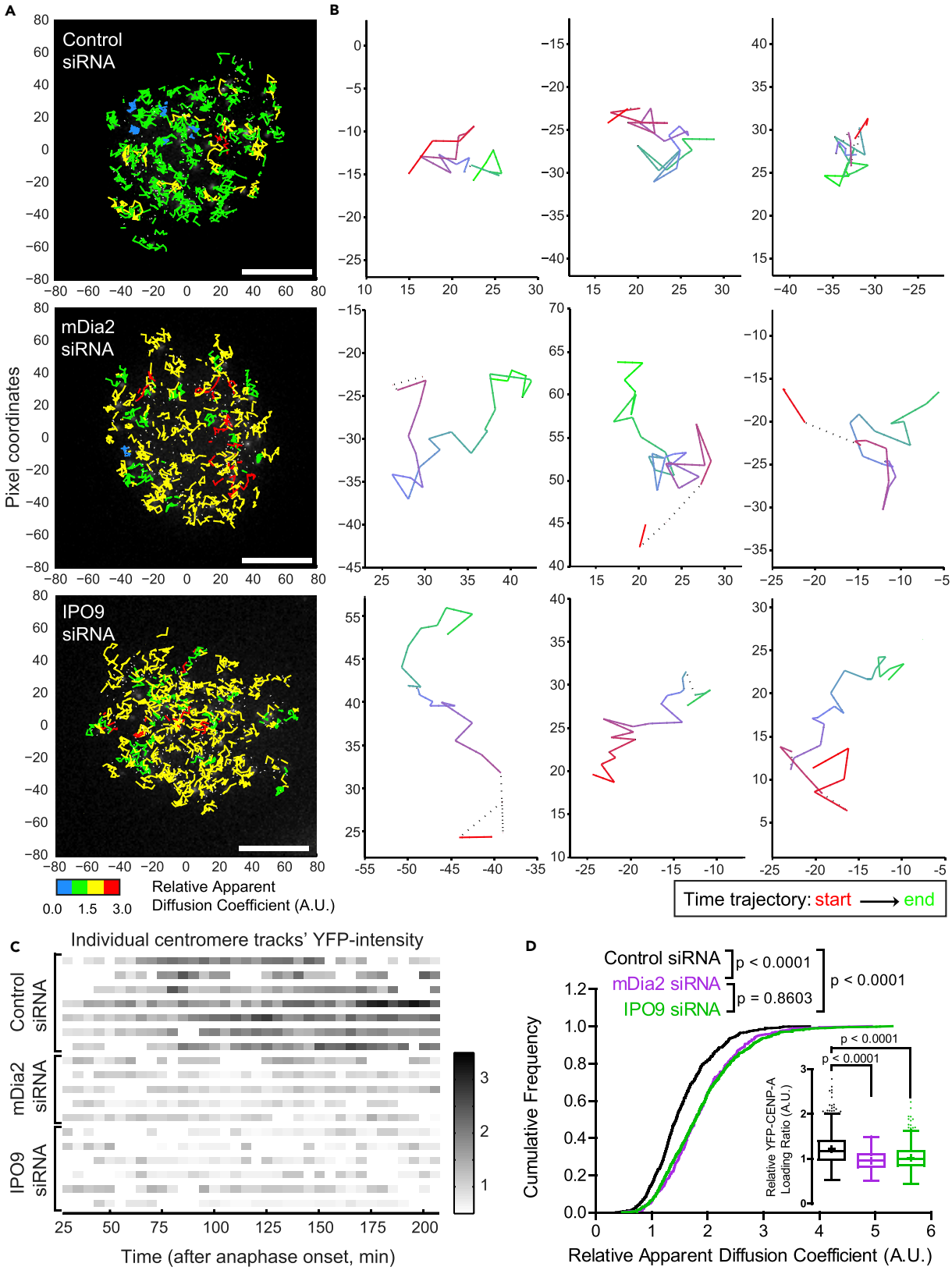
A
B
Control siRNA
mDia2 siRNA
IPO9 siRNA
Pixel coordinates
Relative Apparent Diffusion Coefficient (A.U.)
0.0 1.5 3.0
Time trajectory: start → end
C
Individual centromere tracks' YFP-intensity
Control siRNA
mDia2 siRNA
IPO9 siRNA
Time (after anaphase onset, min)
D
Control siRNA
mDia2 siRNA
IPO9 siRNA
p < 0.0001
p = 0.8603
p < 0.0001
Cumulative Frequency
Relative Apparent Diffusion Coefficient (A.U.)
Relative YFP-CENP-A Loading Ratio (A.U.)

Figure 3. mDia2 and Nuclear Actin Are Required for Subdiffusive Centromere Movement Coinciding with CENP-A Loading in Early G1

(A) A control cell (upper) and cells depleted of mDia2 (middle) or IPO9 (lower) stably expressing YFP-CENP-A in early G1. Color-coded centromere tracks were overlaid on the YFP-CENP-A image from the corresponding video. Centromere tracks were color coded based on their relative apparent diffusion coefficient (blue, low; red, high). Scale bars, 5 μm. See also Video S5.

(B) Representative centromere tracks during early G1 from respective cells on the left in (A). Centromere tracks are color coded based on time: each track starts in red and ends in green. Occasional dotted lines are due to tracking gaps.

(C) Heatmap showing representative centromere-tracks' intensity profiling in early G1. Control, mDia2 knockdown, and IPO9 knockdown are scaled so that their intensity levels at the beginning of the profiling (~25 min after anaphase onset) are comparable. Each horizontal bar is one track spanning from 25 min to 200 min after anaphase onset. Intensity information of YFP-CENP-A tracks at each frame is color coded (lighter gray, low intensity; darker gray, high intensity).

(D) Quantification of the dynamics of centromere movement in early G1. Cumulative frequency was plotted for the relative apparent diffusion coefficients of centromeres in cells transfected with control (GAPDH), mDia2, or IPO9 small interfering RNA (siRNA). The p values were computed using two-tailed t test (Kolmogorov-Smirnov test was also performed with the same statistical conclusions, i.e., $p = 8.7235 \times 10^{-16}$ between control and mDia2 siRNA; $p = 2.9809 \times 10^{-22}$ between control and IPO9 siRNA; $p = 0.3903$ between mDia2 siRNA and IPO9 siRNA). Insets are the Whisker-Tukey boxplots showing the relative YFP-CENP-A loading ratio per track (see Methods for algorithm details). The center bars denote median, and the "+" marks denote mean. The p value for insets was computed using two-tailed t test. Total measurement of 835 (control), 344 (mDia2 siRNA), and 919 (IPO9 siRNA) tracks of centromere movement. See also Figure S3.

Formin mDia2 and Nuclear Actin Are Important for the Relatively Confined Centromere Movement during New CENP-A Loading

Dynamic and short nuclear actin filaments can potentially regulate nuclear events by providing mechanical inputs that either actively transport cargos or help organize nuclear contents. Upon telomere damage, it has been shown that telomere movement is enhanced, which is likely to facilitate DNA repair (Chen et al., 2013; Dimitrova et al., 2008; Wang et al., 2008). To test whether mDia2-mediated nuclear actin polymers affect centromere movement during new CENP-A loading, single-particle tracking of centromere movement was performed in early G1 nuclei by filming HeLa cells stably expressing YFP-CENP-A at relatively high sampling frequency during initial CENP-A loading (Figure 3A and Video S5). Trajectories of these loci in control cells displayed relatively confined movement (Figure 3B), with anomalous diffusion over the timescale of initial CENP-A loading in early G1, about 25–200 min post anaphase onset. The confined centromere motion, however, is significantly impaired upon mDia2 or IPO9 knockdown (Figures 3A, 3B, and S3), with relative apparent diffusion coefficients elevated by 22.1% and 22.6%, respectively (Figure 3D), implying that either mDia2 or IPO9 depletion could be perturbing the same pathway. In particular, long-range centromere movements over the scale of several micrometers were occasionally observed in mDia2 or IPO9 knockdowns but not in control cells (Video S5). Thus the formin mDia2 and nuclear actin are required for the relatively confined movement of centromeres on the timescale of CENP-A loading in early G1. Furthermore, intensity profiling of individual tracks showed that the relative YFP-CENP-A loading ratio in control cells was significantly higher than that in mDia2 or IPO9 knockdown cells (Figures 3C and 3D), supporting that mDia2 and nuclear actin are essential for new CENP-A loading.

MgcRacGAP, like mDia2, Is Required for Apparent CENP-A Loading in Early G1

It has been reported that a small GTPase signaling pathway utilizing the GTPase-activating protein (GAP) MgcRacGAP is essential for the stable maintenance of new CENP-A levels at centromeres (Lagana et al., 2010). We have previously shown that overexpressing a constitutively active fragment of mDia2 can rescue defective CENP-A levels at the centromere caused by MgcRacGAP depletion, suggesting an epistasis where mDia2 could work downstream of MgcRacGAP pathway (Liu and Mao, 2016). However, MgcRacGAP has been observed to have apparent centromere enrichment during late G1 (Lagana et al., 2010), when active new CENP-A loading supposedly has finished. To address this apparent inconsistency, we performed high-resolution ratiometric live cell imaging after directly depleting MgcRacGAP, to examine the temporal requirement of the MgcRacGAP-dependent small GTPase pathway during CENP-A loading. Depleting MgcRacGAP caused apparent CENP-A loading defects in live cells going through early G1 phase: in the absence of MgcRacGAP, the increase in YFP-CENP-A levels at individual centromeres cannot be maintained despite an initial slight increase within 2 hr after anaphase onset (Figures 4A and 4B; Video S6). Non-linear regression using a first-order reaction model predicted a substantially lower plateau (maximum) loading amount that is approximately 50% of the normal loading amount, as well as higher rate constant, consistent with attempted yet failed loading behaviors (Figure 4C). These data agree with the phenotype caused by mDia2 depletion, thus by revealing the temporal requirement of the MgcRacGAP-dependent small GTPase pathway, they support the epistatic relationship between MgcRacGAP and mDia2 in early G1 phase.

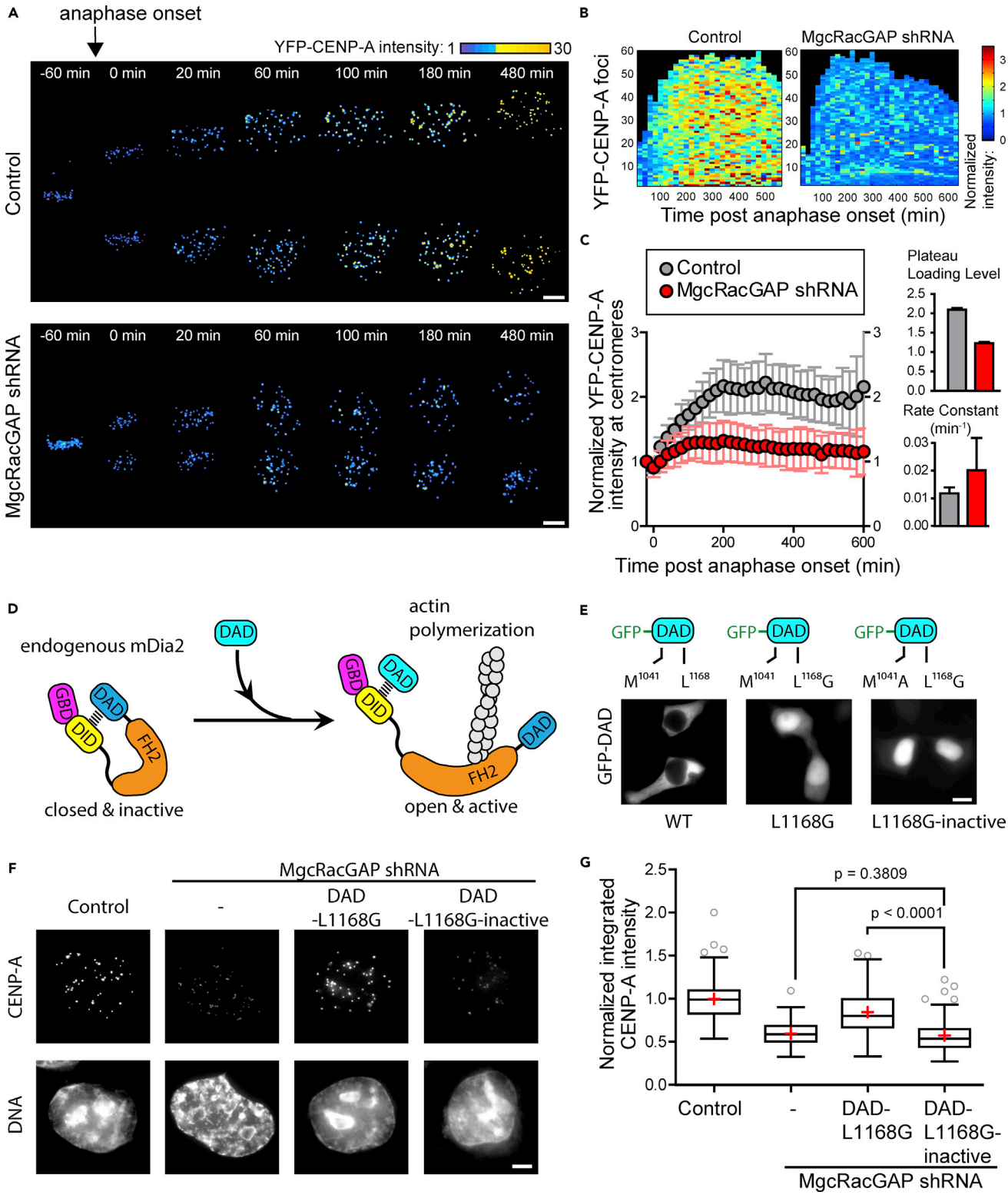

Figure 4. MgcRacGAP-Dependent Signaling Pathway Functions Upstream of Endogenous mDia2 in Early G1 Phase

(A) High-resolution ratiometric live-cell imaging showing unsuccessful YFP-CENP-A loading in early G1 upon MgcRacGAP depletion. The first recorded frames after anaphase onset were aligned to be time point 0 min. Identical lookup table was used over time for both control and MgcRacGAP knockdown. Warmer pseudo-color shows higher levels of YFP-CENP-A. Scale bar, 5 μm. See also Video S6.

Figure 4. *Continued*

(B) Time-lapse heatmap showing the intensity of YFP-CENP-A at each single centromere automatically detected over time in representative control and MgcRacGAP-depleted cells. Each colored box represents one single detected YFP-CENP-A focus, and the color of that box was coded by the normalized intensity of that focus at that particular time point. Due to low sampling frequency, a horizontal trace in the plot may not necessarily indicate the track of the same focus/centromere over time.

(C) Quantification of centromeric YFP-CENP-A levels during G1 phase. Hundreds of centromeres from control or MgcRacGAP knockdown cells (at least 10 cells in each group) were clustered into each cell's average trace before being plotted as ensemble average ± 95% confidence intervals for normalized YFP-CENP-A intensity at centromeres. Plateau loading levels and rate constant were plotted as mean ± SEM.

(D) Schematics of the ectopic activation of endogenous mDia2. Exogenous Dia autoinhibition domain (DAD) fragment of mDia2 can bind to the Dia-interacting domain (DID) of endogenous mDia2 and enable its actin polymerization activity even in the absence of Rho GTPase binding to the GTPase-binding domain (GBD) of endogenous mDia2.

(E) Localization of engineered DAD fragments. Wild-type DAD fragment is extruded from the nucleus, and a point mutation, L1168G, in a nuclear exporting signal (NES)-like motif caused its nuclear accumulation. M1041A is a mutation in the core region that makes the DAD fragment unable to stimulate endogenous mDia2 activation. Scale bar, 10 μm.

(F) Ectopic induction of endogenous mDia2 with DAD-L1168G rescues reduced CENP-A levels caused by MgcRacGAP depletion. Representative immunofluorescence images showing CENP-A levels at centromeres. DNA are stained with DAPI. Scale bar, 5 μm.

(G) Quantification of the normalized CENP-A integrated intensity per nucleus using Whisker-Tukey boxplots. The center bars denote the median, and the + marks denote the mean. The p values were computed using two-tailed t test. Total measurement of 95 (control), 96 (MgcRacGAP short hairpin RNA [shRNA]), 91 (MgcRacGAP shRNA + DAD-L1168G), and 82 (MgcRacGAP + DAD-L1168A-inactive) cells.

Endogenous mDia2 Acts Downstream of the MgcRacGAP-Dependent GTPase Signaling Pathway to Ensure Ordinary CENP-A Levels at Centromeres

To further confirm that endogenous mDia2 indeed functions downstream of the MgcRacGAP-dependent small Rho GTPase molecular switch, we introduced exogenous fragment of the Dia autoinhibition domain (DAD) of mDia2 into cells depleted of MgcRacGAP. DAD fragment can bind to the Dia-interacting domain (DID) of endogenous mDia2 with high affinity, and thus ectopically opens up the otherwise auto-inhibited endogenous mDia2 due to a lack of small Rho GTPase binding to the GTPase-binding domain at the N terminus (Figure 4D) (Kovar, 2006; Palazzo et al., 2001). A point mutation (L1168G) was introduced in the nuclear exporting signal (NES)-like motif of DAD such that this fragment shifts its cytosolic distribution into the nucleus (Baarlink et al., 2013; Miki et al., 2009). Another point mutation (M1141A) at the core of DAD abolishes its interaction with DID (Alberts, 2001), thus the combination of L1168G and M1141A serves as an "inactive" control (Figure 4E). As expected, centromeric CENP-A levels were significantly reduced upon knocking down MgcRacGAP. Importantly, the decrease of CENP-A levels can be rescued by co-expressing DAD-L1168G, but not the DAD-L1168G-inactive fragment (Figures 4F and 4G). Because the DAD fragment per se is not necessary for restoring centromeric CENP-A levels upon depleting endogenous mDia2 (Liu and Mao, 2016), the results here suggest an epistatic relationship between the upstream MgcRacGAP-based small GTPase signaling and downstream endogenous mDia2 in maintaining CENP-A levels at the centromeres.

Centromere Association of HJURP Is Prolonged upon Depleting IPO9 or MgcRacGAP

To further understand how mDia2-mediated nuclear actin polymers, which lie downstream of the MgcRacGAP pathway, affect CENP-A loading, we looked at molecular machineries directly responsible for CENP-A assembly. New CENP-A loading during early G1 requires HJURP, the molecular chaperone with CENP-A nucleosome assembly activity (Barnhart et al., 2011). HJURP transiently localizes to the centromere, and thus only a subset of G1 nuclei have HJURP-positive centromeres (Dunleavy et al., 2009; Foltz et al., 2009). We have previously shown that mDia2 depletion results in higher indices of G1 nuclei with HJURP-positive centromeres, which can be caused by reduced HJUPR turnover, and the prolonged association of HJURP molecules with the centromere could prevent further association of HJURP carrying new CENP-A, thus resulting in CENP-A loading defects (Liu and Mao, 2016). If mDia2 indeed promotes stable CENP-A loading by polymerizing nuclear actin, disrupting nuclear actin would result in similar phenotype regarding HJURP turnover compared with mDia2 depletion. To test this, we depleted IPO9 in synchronized cells stably expressing EGFP-HJURP. Quantitative measurement revealed that the fluorescence intensities of EGFP-HJURP on individual centromeres are not affected upon IPO9 depletion, but the percentage of cells with HJURP-positive centromeres are significantly increased (Figures 5 and S4), a phenotype similar to that of mDia2 depletion. Notably, the increased percentage of cells with HJURP-positive centromeres upon IPO9 depletion are significantly reduced upon co-expressing the NLS-tagged actin, which accumulates in the nucleus independent of IPO9 (Figures 5C and 5D). These data are consistent with a pathway wherein mDia2 promotes stable CENP-A loading via nuclear actin, such that disrupting this pathway results

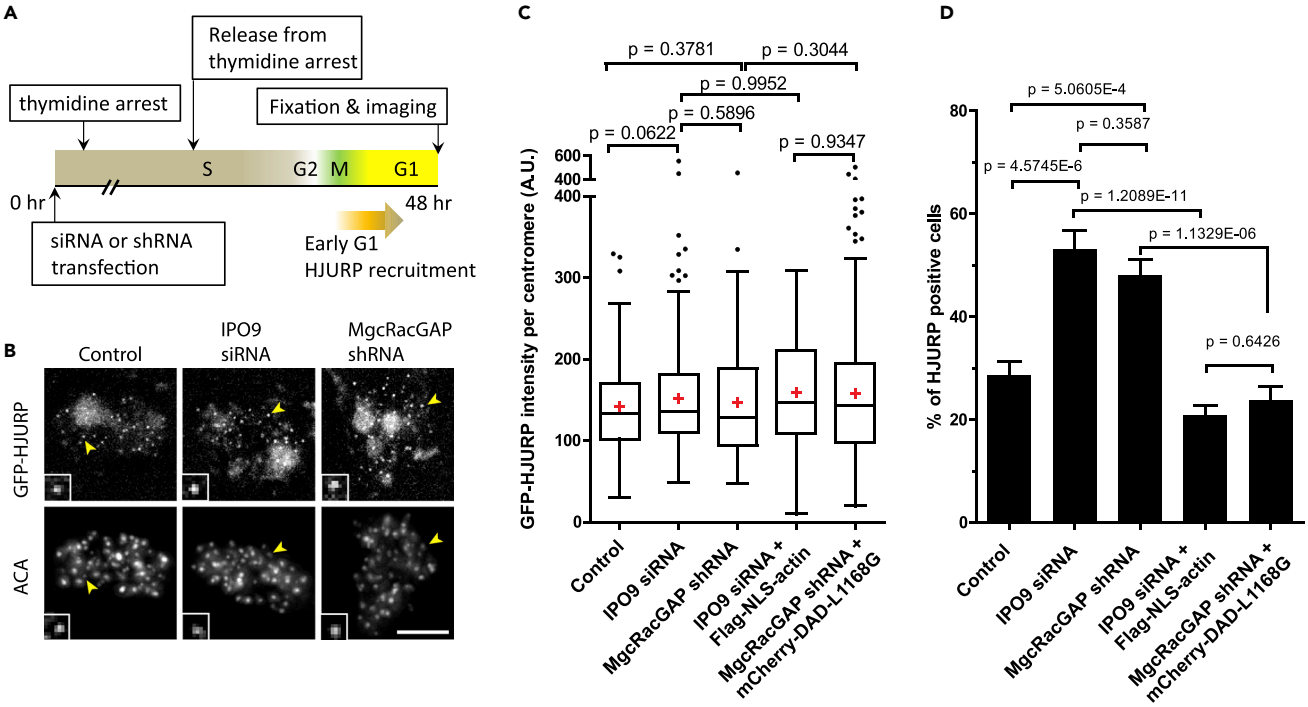

Figure 5. HJURP Localization at Centromeres Is Prolonged upon Depletion of IPO9 or MgcRacGAP

(A) Schematics for depletion and cell synchronization protocols to examine centromere localization of HJURP in early G1 cells.

(B) Representative immunofluorescence images showing GFP-HJURP and centromeres stained with ACA antibodies. Yellow arrowheads point to centromeres shown in insets. Scale bar, 5 μm (insets are 3× magnified). GFP or ACA images are scaled on the identical lookup table over control and depletion groups, respectively. See also Figure S4.

(C) Whisker-Tukey boxplots on the relative intensity of GFP-HJURP foci at centromeres, in cells under different conditions. The center bars denote the median, and the + marks denote the mean. The p values were computed using two-tailed t test. Total measurement of 261 centromeres from 23 cells (control), 267 centromeres from 21 cells (IPO9 small interfering RNA [siRNA]), 102 centromeres from 13 cells (MgcRacGAP short hairpin RNA [shRNA]), 91 centromeres from 13 cells (IPO9 siRNA + FLAG-NLS-actin), and 233 centromeres from 13 cells (MgcRacGAP shRNA + mCherry-DAD-L1168G).

(D) Mean percentages of GFP-HJURP centromere-positive cells under different conditions, with error bars showing SEM from three independent experiments. The p value was computed using a two-tailed z-test. Total measurement of 198 cells (control), 136 cells (IPO9 siRNA), 123 cells (MgcRacGAP shRNA), 368 cells (IPO9 siRNA + FLAG-NLS-actin), and 294 cells (MgcRacGAP shRNA + mCherry-DAD-L1168G).

in prolonged HJURP dwelling and reduced HJURP turnover at the centromere, which lead to defective CENP-A loading (Liu and Mao, 2016). Importantly, the same phenotype of increased percentage of cells with HJURP-positive centromeres was observed by depleting MgcRacGAP, and this phenotype is effectively rescued by co-expressing DAD-L1168G, which ectopically activates endogenous mDia2 even in the absence of MgcRacGAP. These data indicate that mDia2-polymerized nuclear actin functions on the same pathway as the MgcRacGAP-dependent small GTPase signaling to promote stable CENP-A loading via timely HJURP turnover (Lagana et al., 2010) (Figure 6).

DISCUSSION

Faithful transmission of chromosomes during mitosis requires the stable maintenance of centromeres, whose identity is epigenetically defined by a finite number of CENP-A-containing nucleosomes (Bodor et al., 2014). In this work, we show that the cytoskeletal protein formin mDia2 is required for the formation of short dynamic nuclear actin filaments that are enriched in close proximity to centromeres in early G1, and nuclear actin polymers are required for maintaining CENP-A levels at the centromere. Notably, both mDia2 and nuclear actin are important for the relatively constrained centromere movement during CENP-A loading. Also, the lack of nuclear actin or MgcRacGAP results in prolonged centromere association of the CENP-A loading chaperone HJURP, which can be rescued with polymerization-competent NLS-actin or ectopically activated endogenous mDia2, respectively. These results support the idea that formin mDia2, by acting downstream of the MgcRacGAP-dependent signaling pathway, polymerizes short nuclear actin filaments to ensure the stable loading of CENP-A in early G1. This is achieved at least in part by

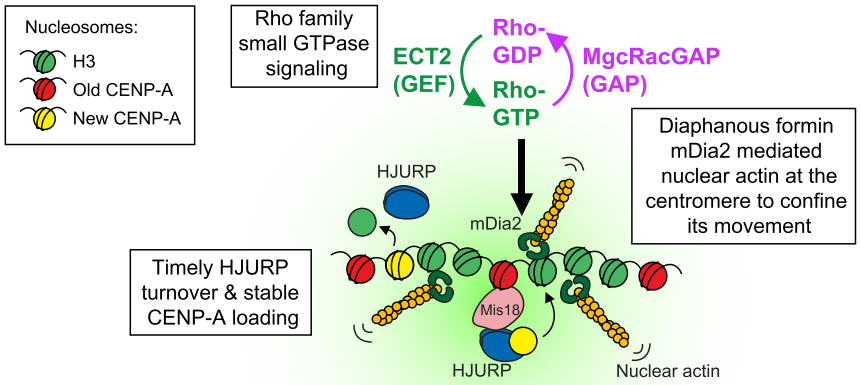

Figure 6. Model for Nuclear Actin Polymerized by mDia2 Promoting Stable CENP-A loading

Formin mDia2 bridges upstream small GTPase signaling with downstream nuclear environment during stable CENP-A loading at the centromeres in early G1. Nuclear actin polymers mediated by mDia2 can help restrict centromere movement during CENP-A loading to ensure the timely turnover of HJURP, contributing to the stable marking of centromeres' epigenetic identities. Some key players in CENP-A loading are annotated in the cartoon.

restricting the movement of centromeres during CENP-A loading so that the HJURP-mediated new CENP-A assembly reactions can be productive. The formin mDia2 therefore connects the upstream MgcRacGAP-dependent signaling pathway to the downstream physicochemical environment at each centromere, to facilitate the stable marking of centromeres' epigenetic identities (Figure 6).

Our results connect mDia2 directly to the upstream signaling pathway that has been shown to stabilize newly loaded CENP-A at the centromeres. A small Rho GTPase signaling pathway has been identified to be essential for stable maintenance of CENP-A levels at the centromeres. Depletion of the GAP MgcRacGAP, the guanine nucleotide exchange factor ECT2, as well as the downstream small GTPases Cdc42 and Rac1 result in 50% reduction of centromeric CENP-A levels (Lagana et al., 2010), suggesting that the small GTPase cycling is important in maintaining centromeric CENP-A. Notably, it has been shown that MgcRacGAP only starts to have obvious centromere localization until late G1 (Lagana et al., 2010). By contrast, mDia2, a candidate effector downstream of the MgcRacGAP-dependent signaling pathway, is required for loading new CENP-A in early G1 (Liu and Mao, 2016). This obvious discrepancy is addressed in this work by the ectopic induction of endogenous mDia2 in the background of MgcRacGAP depletion, as well as by direct live imaging of YFP-CENP-A loading dynamics in the absence of MgcRacGAP. Importantly, our results support an epistatic relationship between MgcRacGAP and mDia2 and reveal that MgcRacGAP is required for CENP-A loading in early G1, consistent with the temporal requirement of mDia2 during CENP-A loading. It is possible that modest levels of MgcRacGAP already exist at early G1 centromere (before its fluorescence signal at the centromere becomes apparently distinguishable from the background) to regulate small Rho GTPase signaling, which then activates mDia2 to polymerize nuclear actin, ensuring stable incorporation of new CENP-A via HJURP. Accordingly, centromeric localization of MgcRacGAP at later G1 could represent a separate function that can be potentially uncovered using temporally resolved optogenetic perturbations (Niopek et al., 2016).

As a downstream effector of the MgcRacGAP-dependent signaling pathway, formin mDia2 can both stabilize microtubules and nucleate linear F-actin (Chesarone et al., 2010). The fact that the K853A mutant of mDia2, while maintaining its microtubule stabilization activity (Bartolini et al., 2008), failed to replace endogenous mDia2 in maintaining CENP-A levels at the centromeres supports the idea that the actin nucleation activity of mDia2 is important for its role in CENP-A loading. Stable maintenance of CENP-A levels at the centromere relies on the nuclear distribution of mDia2 (Liu and Mao, 2016), and our results here indicate that mDia2 is required for the timely appearance of dynamic, short actin filaments inside

the nucleus during the time window when new CENP-A proteins are loaded at centromeres. Depleting nuclear actin by knocking down IPO9 has revealed that nuclear actin itself is important for CENP-A loading at the centromeres. Because actin exists in two pools at equilibrium—the monomer pool and the polymer pool—it has been debated whether actin polymerization inside the nucleus functions by simply depleting the monomer pool, or in contrast, by actually doing mechanical work with the polymerized filaments. The first hypothesis is supported by the observation that actin polymerization inside the nucleus releases the inhibitory effect of monomeric actin on megakaryocytic acute leukemia protein, a cofactor for the transcriptional factor serum response factor (Baarlink et al., 2013; Plessner et al., 2015). However, monomer removal seems not to be the main reason behind the role of nuclear actin polymerization in CENP-A loading. If monomer removal is the primary mechanism required for mDia2-dependent CENP-A loading, knocking down IPO9 (by which both monomer and polymer pools of nuclear actin are depleted [Belin et al., 2015]) would not result in the same phenotypes compared with filament inhibition achieved by mDia2 depletion. Meanwhile, the fact that the NLS-tagged polymerizable actin but not its nonpolymerizable counterpart effectively restored CENP-A levels, and that Utr230-EGFP-NLS-probed nuclear actin polymers is enriched at centromeres, suggests that it is the filament-specific functions that participate in regulating stable CENP-A maintenance. Similar to our findings, it has been shown that the filament-specific functions of nuclear actin are required for efficient clearance of DNA DSBs, although via an mDia1/2-independent but Formin-2-dependent mechanism (Belin et al., 2015). Alongside the different choices of formin proteins in these processes, the polymerized nuclear actin filaments we observed in early G1 cell nuclei have different morphology compared with those observed upon methyl methanesulfonate-induced DNA damage, using the same Utr230-EGFP-NLS probe. On one hand, this implicates a diversified usage of nucleators for actin polymerization involved in different chromosomal functions; on the other hand, as it has been suggested that CENP-A can be recruited to sites of DSB under specific conditions (Zeitlin et al., 2009), it could be interesting to examine the potential link between centromere maintenance and DSB response/repair by testing the role of mDia2-mediated nuclear actin during CENP-A recruitment to DSBs under those specific conditions.

Nuclear actin polymerization has also been recently reported to play important roles during mitotic exit by promoting nuclear volume expansion and chromatin decondensation (Baarlink et al., 2017). Specifically, a transient pool of nuclear F-actin has been visualized by anti-actin chromobody fused with GFP-NLS (nAC-GFP) or by shuttling actin-chromobody (sAC-GFP). These chromobody-visualized filaments appear right after daughter cell nuclei reformation (within about 7 min after anaphase) and persist for 60–70 min in early G1 nuclei before being disassembled. What we observed here using the Utr230-EGFP-NLS nuclear actin probe appeared different from the chromobody-visualized nuclear actin filaments in several ways. First, the typical lengths of nuclear actin filaments visualized by chromobodies are over several micronmeters, and such morphology was not observed with Utr230-EGFP-NLS upon mitotic exit. Second, the typical time window for the initial observation of nuclei with Utr230-EGFP-NLS puncta is much delayed than that with chromobody-labeled filaments. Third, the total duration for nuclear punctate Utr230-EGFP-NLS signals to be present in a nucleus is much longer than that for nuclear chromobody-labeled filaments and covers the bulk of time spent on CENP-A loading (Liu and Mao, 2016). Therefore, what we observed here could reflect a different pool of nuclear actin polymers that appear later but persist longer to facilitate CENP-A loading. Indeed, it has been shown that the chromobody-visualized actin filaments in early G1 is regulated by cofilin but not mDia2, whereas we show here that the Utr230-EGFP-NLS-visualized puncta in G1 require mDia2. Furthermore, nuclear volume expansion, as a proposed role of the chromobody-visualized actin filaments, is sensitive to cytochalasin D and latrunculin B, whereas Utr230-EGFP-NLS-visualized puncta remain inert to those drugs (Belin et al., 2013) and CENP-A levels at centromeres remain the same after treatment by cytochalasin or latrunculin (Lagana et al., 2010). It remains interesting to examine the spatiotemporal relationship between the nuclear actin polymers visualized by chromobodies and those by Utr230-EGFP-NLS, especially in the presence of fluorescently labeled centromere markers in live cells going through G1 phase.

Short and dynamic nuclear actin filaments can potentially regulate nuclear processes through two major mechanisms that involve mechanical work: (1) modulating the mobility or organization of chromatins and (2) delivering other assembly factors essential for CENP-A loading, or sequestering inhibitory factors that would otherwise suppress CENP-A loading. These two scenarios are not mutually exclusive. Although a sequestering role is consistent with a lack of obvious localization of mDia2 at the centromere, further biochemical experiments are needed to examine potential interactomes of mDia2 in G1 nuclei. A role in

delivering assembly factors is inconsistent with the fact that at least the recruitment of HJURP at G1 centromeres is not affected upon the depletion of mDia2 (Liu and Mao, 2016), IPO9, or MgcRacGAP. Finally, a role in regulating the movement or spatial organization of chromosome/chromatin is supported by the apparent change in the subdiffusive behaviors of centromeres upon mDia2 or IPO9 knockdown, correlated with defective CENP-A loading. The subdiffusive motion itself is consistent with the hypothesized local reaction chambers that greatly enhance chemical efficiency (Robson et al., 2012). Physically, this phenomenon is consistent with relatively stable chromosome territories (Gerlich et al., 2003) and the fractal globule model (Mirny, 2011), in particular the quickly reestablished chromosomal long-range *cis*-contacts and the topologically associated domain insulation in early G1 (Nagano et al., 2017). Indeed, we have observed several long-range centromere movements in mDia2- or IPO9-depleted cells (Video S5). Whether these observations reflect perturbed, global changes in chromosomal organizations or mobility in mDia2- or IPO9-depleted cells remains to be investigated, and one potential future direction is to use live imaging to track other chromosome regions marked by the *lacO*/LacI-GFP system (Ding and Hiraoka, 2017) or the GFP-tagged endonuclease-deficient Cas9 (dCas9) system (Chen et al., 2013). Meanwhile, the confined movement of centromeric chromatin is consistent with recent findings that heterochromatin-rich areas inside the nucleus show less movement compared with other chromosomal domains (Nozaki et al., 2017). Heterochromatin domain formation is mediated by phase separation of heterochromatin proteins including HP1α (Larson et al., 2017; Strom et al., 2017), which colocalizes with CENP-A at the centromere (Bártová et al., 2005). It remains to be examined whether formin-mediated nuclear actin network affects the liquid properties exhibited by heterochromatin domains. In addition, it remains to be tested whether the movement of centromeres per se affects CENP-A loading, potentially by perturbing phase separation that occurs at centromeric heterochromatin (Shin et al., 2017; Strom et al., 2017), or by ectopically moving centromeres with optogenetic tools (Ballister et al., 2014; Zhang et al., 2017).

The epigenetic inheritance of chromosomal landscapes in eukaryotes often requires the integration of signaling pathways and spatial organization in the nucleus (Bickmore and van Steensel, 2013). Collectively, our results suggest a mode of regulation where nuclear actin polymerized by formin mDia2 contributes to the physical confinement of early G1 centromeres, and such confinement is essential for the efficient HJURP-mediated assembly reactions of new CENP-A. Formin mDia2 therefore could function as a link between upstream small GTPase signaling and the downstream viscoelastic local environment surrounding centromeres, to regulate the stable marking of centromere's epigenetic identity. Given the many recently identified chromatin-associated biomolecular condensates that phase-separate from the rest of the nucleus (Cho et al., 2018; Chong et al., 2018; Plys and Kingston, 2018; Sabari et al., 2018), it is intriguing to speculate whether the motion-restricted G1 centromeres and the associated nuclear actin puncta are part of certain phase-separated condensates that provide an organization necessary for productive nucleosome assembly reactions.

Limitations of the Study

Although the present evidence suggests that disruption of cargos of IPO9 other than actin is not likely to play a role in causing defective CENP-A loading, direct examination of other factors (such as HJURP) would be required to conclusively rule out side effects of IPO9 depletion. YFP-CENP-A is the only fluorescently labeled centromere marker available in hand for live imaging, thus rescue experiments for the centromere movement assay are currently not possible due to the lack of additional fluorescent centromere markers. Finally, although the present data provide some insight into a potential epistatic relationship between MgcRacGAP and mDia2, additional investigation is required to identify the exact mechanisms involved.

METHODS

All methods can be found in the accompanying Transparent Methods supplemental file.

SUPPLEMENTAL INFORMATION

Supplemental Information includes Transparent Methods, four figures, two tables, and six videos and can be found with this article online at https://doi.org/10.1016/j.isci.2018.10.031.

ACKNOWLEDGMENTS

We thank all members of the Mao laboratory for stimulating discussion. We thank Gregg Gundersen and Francesca Bartolini for insights on the project. We thank Richard Vallee, Fred Chang, Julie Canman, and

Abby Dernburg (UC Berkeley) for inputs on the project. We are grateful to Dan Foltz (Northwestern), Dyche Mullins (UCSF), Yuh Nung Jan (UCSF), Abby Dernburg (UC Berkeley), and the late Michael Davidson (National High Magnetic Field Laboratory) for reagents and equipment. We are especially thankful to Justin Salat and Terri Lee (UCSF) for providing the Utr230-EGFP-NLS stable cell line, and Weiguo Zhang (Lawrence Berkeley National Lab) and Bill Brinkley (Baylor College of Medicine) for ACA antibodies. We are also grateful to Yu He (Stanford), Yan Wang (Microsoft), and David Odde (University of Minnesota) for insightful discussions on physics and computational methods. This work has been supported by grants from the National Institutes of Health (GM89768) to Y.M. C.L. is a Walter Group Fellow of the Life Sciences Research Foundation.

AUTHOR CONTRIBUTIONS

C.L., conceptualization and design of experiments, cloning and tissue culture, data acquisition, quantitative imaging and MATLAB programming for image processing, data analysis and interpretation, drafting and revising of the manuscript; R.Z., design of experiments, tissue culture, quantitative imaging, data analysis, and revising the manuscript; Y.M., funding acquisition, conceptualization, data interpretation, and revising the manuscript.

DECLARATION OF INTERESTS

The authors declare no competing interests.

Received: May 3, 2018
Revised: October 4, 2018
Accepted: October 29, 2018
Published: November 30, 2018

REFERENCES

Alberts, A.S. (2001). Identification of a carboxyl-terminal diaphanous-related formin homology protein autoregulatory domain. J. Biol. Chem. *276*, 2824–2830.

Andrin, C., and Hendzel, M.J. (2004). F-actin-dependent insolubility of chromatin-modifying components. J. Biol. Chem. *279*, 25017–25023.

Baarlink, C., Plessner, M., Sherrard, A., Morita, K., Misu, S., Virant, D., Kleinschnitz, E.-M., Harniman, R., Alibhai, D., Baumeister, S., et al. (2017). A transient pool of nuclear F-actin at mitotic exit controls chromatin organization. Nat. Cell Biol. *19*, 1389–1399.

Baarlink, C., Wang, H., and Grosse, R. (2013). Nuclear actin network assembly by formins regulates the SRF coactivator MAL. Science *340*, 864–867.

Ballister, E.R., Aonbangkhen, C., Mayo, A.M., Lampson, M.A., and Chenoweth, D.M. (2014). Localized light-induced protein dimerization in living cells using a photocaged dimerizer. Nat. Commun. *5*, 5475.

Barnhart, M.C., Kuich, P.H.J.L., Stellfox, M.E., Ward, J.A., Bassett, E.A., Black, B.E., and Foltz, D.R. (2011). HJURP is a CENP-A chromatin assembly factor sufficient to form a functional de novo kinetochore. J. Cell Biol. *194*, 229–243.

Bartolini, F., Moseley, J.B., Schmoranzer, J., Cassimeris, L., Goode, B.L., and Gundersen, G.G. (2008). The formin mDia2 stabilizes microtubules independently of its actin nucleation activity. J. Cell Biol. *181*, 523–536.

Bártová, E., Pacherník, J., Harničarová, A., Kovařík, A., Kovaříková, M., Hofmanová, J., Skalníková, M., Kozubek, M., and Kozubek, S. (2005). Nuclear levels and patterns of histone H3 modification and HP1 proteins after inhibition of histone deacetylases. J. Cell Sci. *118*, 5035–5046.

Belin, B.J., Cimini, B.A., Blackburn, E.H., and Mullins, R.D. (2013). Visualization of actin filaments and monomers in somatic cell nuclei. Mol. Biol. Cell *24*, 982–994.

Belin, B.J., Lee, T., and Mullins, R.D. (2015). DNA damage induces nuclear actin filament assembly by Formin-2 and Spire-1/2 that promotes efficient DNA repair. Elife *4*, e07735.

Bickmore, W.A., and van Steensel, B. (2013). Genome architecture: domain organization of interphase chromosomes. Cell *152*, 1270–1284.

Bodor, D.L., Mata, J.F., Sergeev, M., David, A.F., Salimian, K.J., Panchenko, T., Cleveland, D.W., Black, B.E., Shah, J.V., and Jansen, L.E.T. (2014). The quantitative architecture of centromeric chromatin. Elife *3*, e02137.

Chen, B., Gilbert, L.A., Cimini, B.A., Schnitzbauer, J., Zhang, W., Li, G.-W., Park, J., Blackburn, E.H., Weissman, J.S., Qi, L.S., et al. (2013). Dynamic imaging of genomic loci in living human cells by an optimized CRISPR/Cas system. Cell *155*, 1479–1491.

Chesarone, M.A., DuPage, A.G., and Goode, B.L. (2010). Unleashing formins to remodel the actin and microtubule cytoskeletons. Nat. Rev. Mol. Cell Biol *11*, 62–74.

Cho, W.-K., Spille, J.-H., Hecht, M., Lee, C., Li, C., Grube, V., and Cisse, I.I. (2018). Mediator and RNA polymerase II clusters associate in transcription-dependent condensates. Science *361*, 412–415.

Chong, S., Dugast-Darzacq, C., Liu, Z., Dong, P., Dailey, G.M., Cattoglio, C., Heckert, A., Banala, S., Lavis, L., Darzacq, X., et al. (2018). Imaging dynamic and selective low-complexity domain interactions that control gene transcription. Science *361*, eaar2555.

Cleveland, D.W., Mao, Y., and Sullivan, K.F. (2003). Centromeres and kinetochores: from epigenetics to mitotic checkpoint signaling. Cell *112*, 407–421.

Daou, P., Hasan, S., Breitsprecher, D., Baudelet, E., Camoin, L., Audebert, S., Goode, B.L., and Badache, A. (2014). Essential and nonredundant roles for Diaphanous formins in cortical microtubule capture and directed cell migration. Mol. Biol. Cell *25*, 658–668.

Dimitrova, N., Chen, Y.C., Spector, D.L., and de Lange, T. (2008). 53BP1 promotes non-homologous end joining of telomeres by increasing chromatin mobility. Nature *456*, 524–528.

Ding, D.-Q., and Hiraoka, Y. (2017). Visualization of a specific genome locus by the lacO/LacI-GFP system. Cold Spring Harb. Protoc. 804–809.

Dopie, J., Skarp, K.-P., Kaisa Rajakylä, E., Tanhuanpää, K., and Vartiainen, M.K. (2012). Active maintenance of nuclear actin by importin 9 supports transcription. Proc. Natl. Acad. Sci. U S A *109*, E544–E552.

Dundr, M., Ospina, J.K., Sung, M.-H., John, S., Upender, M., Ried, T., Hager, G.L., and Matera, A.G. (2007). Actin-dependent intranuclear

repositioning of an active gene locus in vivo. J. Cell Biol. *179*, 1095–1103.

Dunleavy, E.M., Roche, D., Tagami, H., Lacoste, N., Ray-Gallet, D., Nakamura, Y., Daigo, Y., Nakatani, Y., and Almouzni-Pettinotti, G. (2009). HJURP is a cell-cycle-dependent maintenance and deposition factor of CENP-A at centromeres. Cell *137*, 485–497.

Foltz, D.R., Jansen, L.E.T., Bailey, A.O., Yates, J.R., III, Bassett, E.A., Wood, S., Black, B.E., and Cleveland, D.W. (2009). Centromere-specific assembly of CENP-A nucleosomes is mediated by HJURP. Cell *137*, 472–484.

Fujita, Y., Hayashi, T., Kiyomitsu, T., Toyoda, Y., Kokubu, A., Obuse, C., and Yanagida, M. (2007). Priming of centromere for CENP-A recruitment by human hMis18α, hMis18β, and M18BP1. Dev. Cell *12*, 17–30.

Gerlich, D., Beaudouin, J., Kalbfuss, B., Daigle, N., Eils, R., and Ellenberg, J. (2003). Global chromosome positions are transmitted through mitosis in mammalian cells. Cell *112*, 751–764.

Gonsior, S.M., Platz, S., Buchmeier, S., Scheer, U., Jockusch, B.M., and Hinssen, H. (1999). Conformational difference between nuclear and cytoplasmic actin as detected by a monoclonal antibody. J. Cell Sci. *112*, 797–809.

Jansen, L.E.T., Black, B.E., Foltz, D.R., and Cleveland, D.W. (2007). Propagation of centromeric chromatin requires exit from mitosis. J. Cell Biol. *176*, 795–805.

Kovar, D.R. (2006). Molecular details of formin-mediated actin assembly. Curr. Opin. Cell Biol. *18*, 11–17.

Lagana, A., Dorn, J.F., De Rop, V., Ladouceur, A.-M., Maddox, A.S., and Maddox, P.S. (2010). A small GTPase molecular switch regulates epigenetic centromere maintenance by stabilizing newly incorporated CENP-A. Nat. Cell Biol. *12*, 1186–1193.

Larson, A.G., Elnatan, D., Keenen, M.M., Trnka, M.J., Johnston, J.B., Burlingame, A.L., Agard, D.A., Redding, S., and Narlikar, G.J. (2017). Liquid droplet formation by HP1α suggests a role for phase separation in heterochromatin. Nature *547*, 236–240.

Liu, C., and Mao, Y. (2016). Diaphanous formin mDia2 regulates CENP-A levels at centromeres. J. Cell Biol. *213*, 415–424.

Liu, C., and Mao, Y. (2017). Formin-mediated epigenetic maintenance of centromere identity. Small GTPases *8*, 245–250.

Maddox, P.S., Hyndman, F., Monen, J., Oegema, K., and Desai, A. (2007). Functional genomics identifies a Myb domain–containing protein family required for assembly of CENP-A chromatin. J. Cell Biol. *176*, 757–763.

McDonald, D., Carrero, G., Andrin, C., de Vries, G., and Hendzel, M.J. (2006). Nucleoplasmic β-actin exists in a dynamic equilibrium between low-mobility polymeric species and rapidly diffusing populations. J. Cell Biol. *172*, 541–552.

McKinley, K.L., and Cheeseman, I.M. (2014). Polo-like kinase 1 licenses CENP-A deposition at centromeres. Cell *158*, 397–411.

Miki, T., Okawa, K., Sekimoto, T., Yoneda, Y., Watanabe, S., Ishizaki, T., and Narumiya, S. (2009). mDia2 shuttles between the nucleus and the cytoplasm through the importin-α/β- and CRM1-mediated nuclear transport mechanism. J. Biol. Chem. *284*, 5753–5762.

Mirny, L.A. (2011). The fractal globule as a model of chromatin architecture in the cell. Chromosome Res. *19*, 37–51.

Moree, B., Meyer, C.B., Fuller, C.J., and Straight, A.F. (2011). CENP-C recruits M18BP1 to centromeres to promote CENP-A chromatin assembly. J. Cell Biol. *194*, 855–871.

Nagano, T., Lubling, Y., Várnai, C., Dudley, C., Leung, W., Baran, Y., Mendelson Cohen, N., Wingett, S., Fraser, P., and Tanay, A. (2017). Cell-cycle dynamics of chromosomal organization at single-cell resolution. Nature *547*, 61–67.

Niopek, D., Wehler, P., Roensch, J., Eils, R., and Di Ventura, B. (2016). Optogenetic control of nuclear protein export. Nat. Commun. *7*, 10624.

Nozaki, T., Imai, R., Tanbo, M., Nagashima, R., Tamura, S., Tani, T., Joti, Y., Tomita, M., Hibino, K., Kanemaki, M.T., et al. (2017). Dynamic organization of chromatin domains revealed by super-resolution live-cell imaging. Mol. Cell *67*, 282–293.e7.

Palazzo, A.F., Cook, T.A., Alberts, A.S., and Gundersen, G.G. (2001). mDia mediates Rho-regulated formation and orientation of stable microtubules. Nat. Cell Biol. *3*, 723–729.

Parisis, N., Krasinska, L., Harker, B., Urbach, S., Rossignol, M., Camasses, A., Dewar, J., Morin, N., and Fisher, D. (2017). Initiation of DNA replication requires actin dynamics and formin activity. EMBO J. *36*, 3212–3231.

Plessner, M., Melak, M., Chinchilla, P., Baarlink, C., and Grosse, R. (2015). Nuclear F-actin formation and reorganization upon cell spreading. J. Biol. Chem. *290*, 11209–11216.

Plys, A.J., and Kingston, R.E. (2018). Dynamic condensates activate transcription. Science *361*, 329.

Posern, G., Sotiropoulos, A., and Treisman, R. (2002). Mutant actins demonstrate a role for unpolymerized actin in control of transcription by serum response factor. Mol. Biol. Cell *13*, 4167–4178.

Rando, O.J., Zhao, K., Janmey, P., and Crabtree, G.R. (2002). Phosphatidylinositol-dependent actin filament binding by the SWI/SNF-like BAF chromatin remodeling complex. Proc. Natl. Acad. Sci. U S A *99*, 2824–2829.

Robson, A., Burrage, K., and Leake, M.C. (2012). Inferring diffusion in single live cells at the single-molecule level. Philos. Trans. R. Soc. Lond. B Biol. Sci. *368*, 20120029.

Sabari, B.R., Dall'Agnese, A., Boija, A., Klein, I.A., Coffey, E.L., Shrinivas, K., Abraham, B.J., Hannett, N.M., Zamudio, A.V., Manteiga, J.C., et al. (2018). Coactivator condensation at super-enhancers links phase separation and gene control. Science *361*, eaar3958.

Schoenenberger, C.A., Buchmeier, S., Boerries, M., Sütterlin, R., Aebi, U., and Jockusch, B.M. (2005). Conformation-specific antibodies reveal distinct actin structures in the nucleus and the cytoplasm. J. Struct. Biol. *152*, 157–168.

Serebryannyy, L.A., Cruz, C.M., and de Lanerolle, P. (2016). A role for nuclear actin in HDAC 1 and 2 regulation. Sci. Rep. *6*, 28460.

Shin, Y., Berry, J., Pannucci, N., Haataja, M.P., Toettcher, J.E., and Brangwynne, C.P. (2017). Spatiotemporal control of intracellular phase transitions using light-activated optoDroplets. Cell *168*, 159–171.e14.

Silva, M.C., Bodor, D.L., Stellfox, M.E., Martins, N.M., Hochegger, H., Foltz, D.R., and Jansen, L.E. (2012). Cdk activity couples epigenetic centromere inheritance to cell cycle progression. Dev. Cell *22*, 52–63.

Strom, A.R., Emelyanov, A.V., Mir, M., Fyodorov, D.V., Darzacq, X., and Karpen, G.H. (2017). Phase separation drives heterochromatin domain formation. Nature *547*, 241–245.

Wang, X., Kam, Z., Carlton, P.M., Xu, L., Sedat, J.W., and Blackburn, E.H. (2008). Rapid telomere motions in live human cells analyzed by highly time-resolved microscopy. Epigenetics Chromatin *1*, 4.

Wang, Y.-H., Hariharan, A., Bastianello, G., Toyama, Y., Shivashankar, G.V., Foiani, M., and Sheetz, M.P. (2017). DNA damage causes rapid accumulation of phosphoinositides for ATR signaling. Nat. Commun. *8*, 2118.

Zeitlin, S.G., Baker, N.M., Chapados, B.R., Soutoglou, E., Wang, J.Y.J., Berns, M.W., and Cleveland, D.W. (2009). Double-strand DNA breaks recruit the centromeric histone CENP-A. Proc. Natl. Acad. Sci. U S A *106*, 15762–15767.

Zhang, H., Aonbangkhen, C., Tarasovetc, E.V., Ballister, E.R., Chenoweth, D.M., and Lampson, M.A. (2017). Optogenetic control of kinetochore function. Nat. Chem. Biol. *13*, 1096–1101.

ISCI, Volume *9*

Supplemental Information

Nuclear Actin Polymerized by mDia2 Confines Centromere Movement during CENP-A Loading

Chenshu Liu, Ruijun Zhu, and Yinghui Mao

SUPPLEMENTAL INFORMATION

SUPPLEMENTAL FIGURES

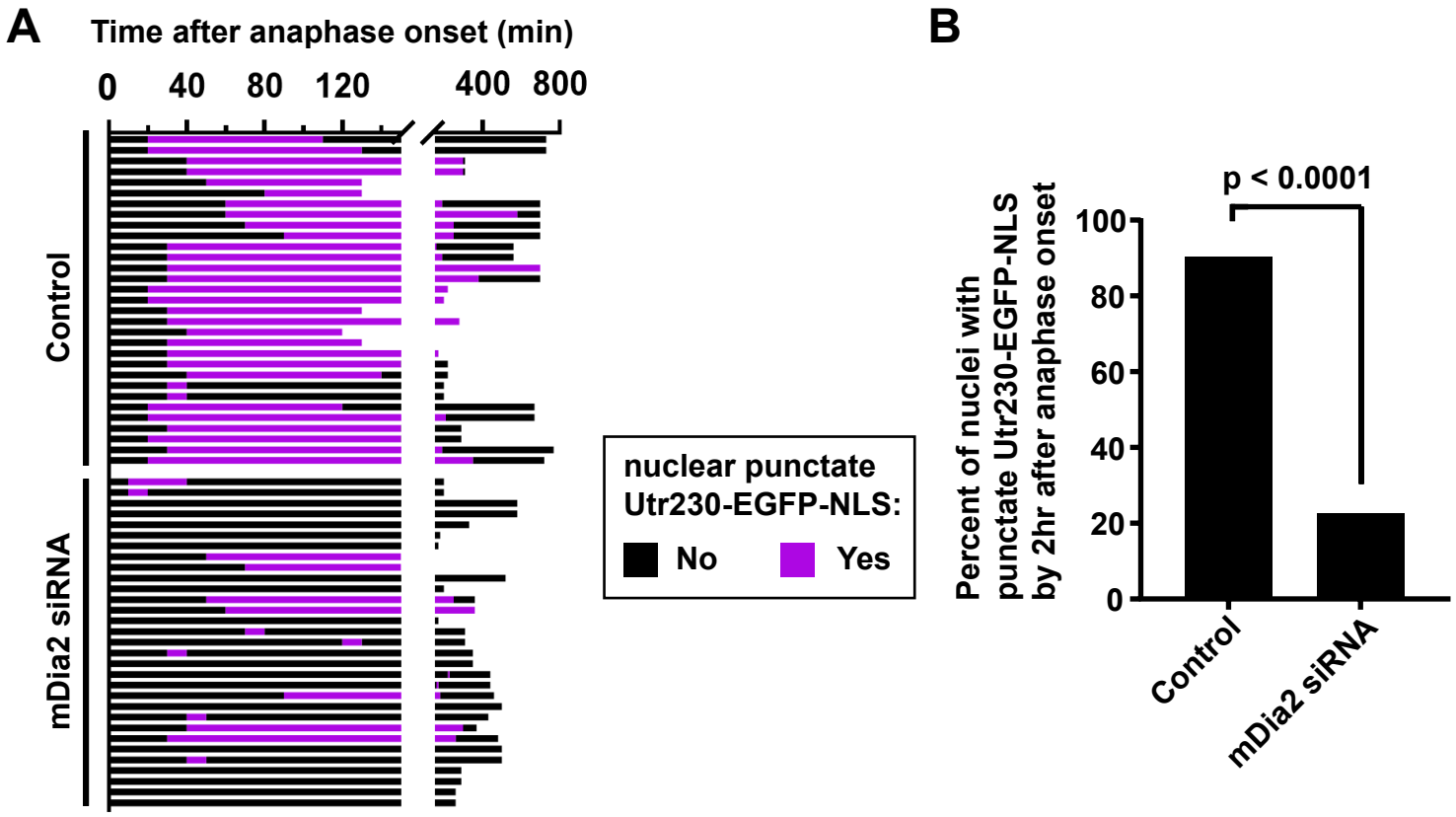

Figure S1 (related to Figure 1). Occurrence and duration of nuclear punctate Utr230-EGFP-NLS are reduced in mDia2 knockdown cells.

(A) Individual cells' trajectories showing the duration of time where nuclear punctate Utr230-EGFP-NLS was present or absent since anaphase onset. Black, punctate Utr230-EGFP-NLS absent; Magenta, punctate Utr230-EGFP-NLS present.

(B) Percentage of nuclei with punctate Utr230-EGFP-NLS by 2hr after anaphase onset. P-value was computed using Fisher's exact test. Total measurement of 31 control cells and 31 mDia2 knockdown cells.

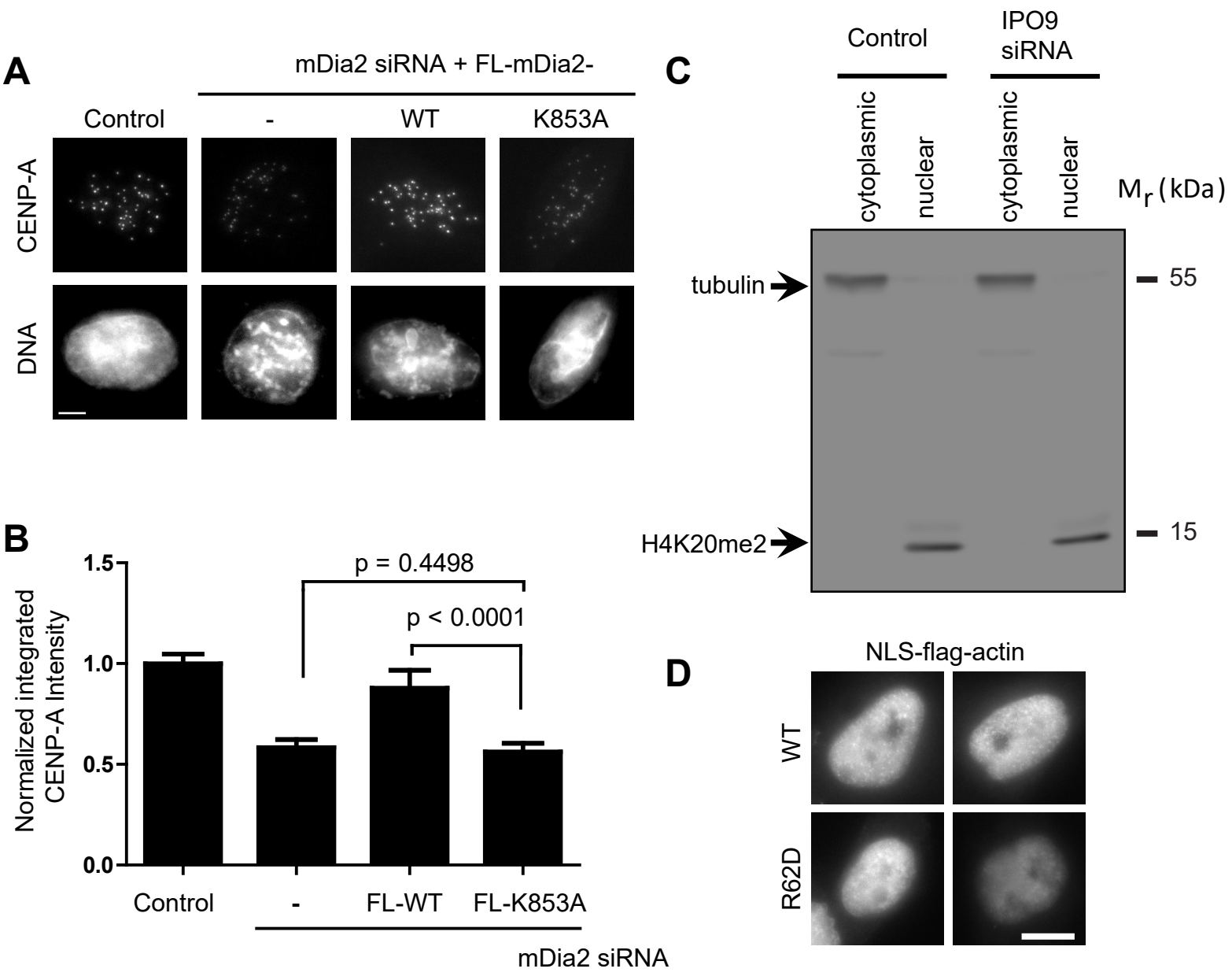

Figure S2 (related to Figure 2). Full length mDia2 with actin polymerization mutation fail to rescue CENP-A levels upon depleting endogenous mDia2 and actin polymerization inside the G1 nucleus.
(A) Representative immunofluorescence images showing CENP-A levels at centromeres. DNA was stained with DAPI. CENP-A images were scaled on the identical look up table over control and experimental conditions. Scale bar, 5 μm.
(B) Quantification of the normalized CENP-A integrated intensity per nucleus. Bar graphs show mean ± 95%confidence interval of each group. The p-values were computed using two-tailed *t* test. Total measurement of 45 (Control), 42 (mDia2 siRNA), 36 (mDia2 siRNA + FL-WT), and 39 (mDia2 siRNA + FL-K853A) cells.
(C) Immunoblot showing marker protein species in the cellular fractionation assay. Tubulin was used to mark the cytoplasmic fraction while H4K20me2 for the nuclear fraction.
(D) Nuclear localization signal (NLS) and flag-tagged actin localize inside the G1 nuclei depleted of IPO9. Flag staining showing the existence of punctate short filaments of WT-actin, but not the non-polymerizable R62D-actin, inside G1 nucleus. Scale bar, 10 μm.

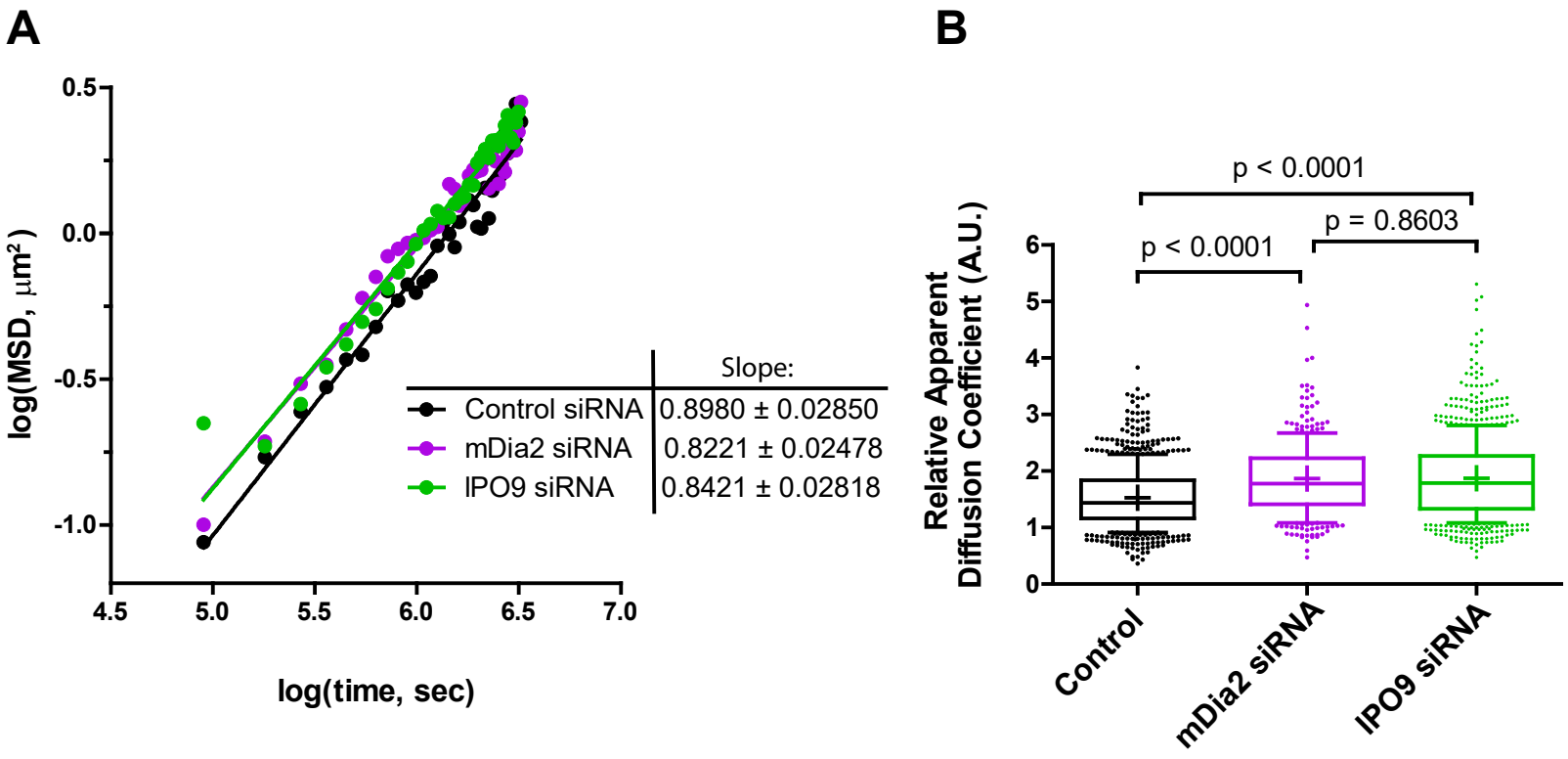

Figure S3 (related to Figure 3). Relatively confined centromere motion depends on mDia2 and nuclear actin.
(A) Log-log plot of ensemble average of MSD versus time (36 time lags for each group) from pooled single particle tracking of centromere movement in early G1 control (GAPDH), mDia2 and IPO9 knockdowns. Overlaid solid lines indicate linear regression (least-square fit, R^2 = 0.9669 (ctrl), = 0.9700 (mDia2 siRNA), = 0.9633(IPO9 siRNA)). Y-intercepts reflect apparent diffusion coefficient, while the slopes indicate the type of diffusion (i.e. anomalous diffusion here). Consistently, ensemble MSD curves (data not shown) demonstrate that MSD appear to saturate with a slightly concave curvature, indicative of impeded movement (anomalous diffusion) rather than free diffusion or directed transportation.
(B) Boxplots showing the normalized apparent diffusion coefficient of G1 centromeres in control, mDia2 and IPO9 knockdown cells (the same data in Figure 3D). The boxes span 10-90 percentile of the data, while the center bars denote median and the '+' marks denote mean. The p-value was computed using two-tailed *t* test.

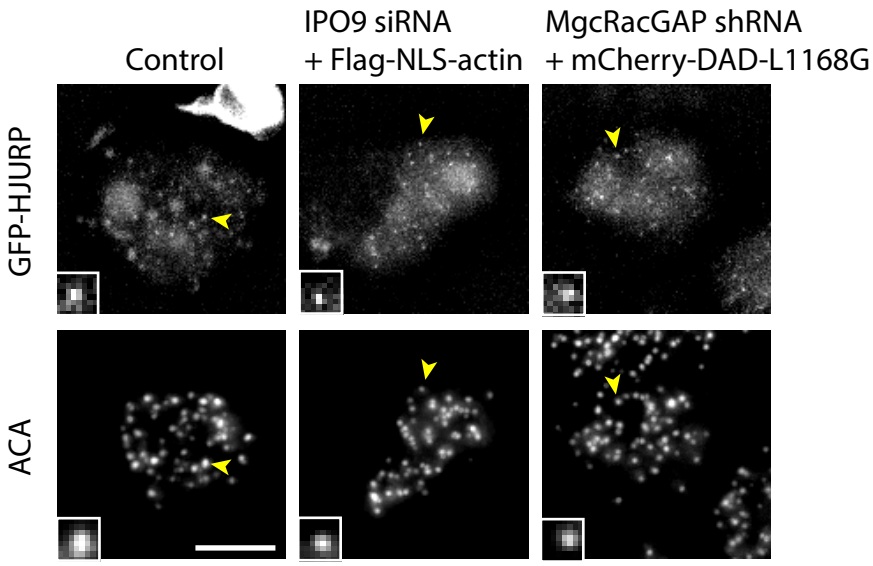

Figure S4 (related to Figure 5). GFP-HJURP localization at centromeres under indicated conditions.
Representative immunofluorescence images showing GFP-HJURP and centromeres stained with ACA antibodies. Yellow arrowheads point to centromeres shown in insets. Scale bar, 5 μm (insets are 3× magnified). GFP or ACA images are scaled on the identical look up table over control and depletion/rescue groups respectively. Rescued cells in the depletion background were identified with Flag or mCherry immunofluorescence as co-transfection markers.

SUPPLEMENTAL TABLES

Table S1. Plasmid constructs used in this study. Related to Figure 1 – 5, S2 and S4.

Plasmid	Source
Utr230-EGFP-NLS	Dyche Mullins (Belin et al., 2013)
NLS-flag-actin	Robert Grosse (Baarlink et al., 2013; Posern et al., 2002)
NLS-flag-actin-R62D	This study
Full length mDia2 (mEmerald-mDia2-C-14)	Michael Davidson (plasmid 54158; Addgene)
Full length mDia2-K853A	This study
GFP-DAD	Gregg Gundersen (Palazzo et al., 2001)
GFP-DAD-L1168G	This study
GFP-DAD-L1168G-M1041A (inactive)	This study
mCherry-DAD-L1168G	This study (pmCherry-C1 as vector)

Table S2. Oligonucleotide target sequences used in this study. Related to Figure 1 – 5, S1 – S4.

Target gene name	Target sequence	Source
human GAPDH	5’-TGGTTTACATGTTCCAATA-3’	(Liu and Mao, 2016)
human mDia2	5’- CTCCGGCACAATTCAGTTCAA-3’	(Liu and Mao, 2016)
human IPO9	5’-ATGGGTTGAGAGAATCGATAA-3’	This study
human MgcRacGAP	5' - CAGGTGGATGTAGAGATCAAA -3'	(Liu and Mao, 2016)

TRANSPARENT METHODS

Constructs, siRNA sequences and antibodies

All constructs used in this study and target sequence information can be found in Table S1 and S2. Utr230-EGFP-NLS was a kind gift from Dyche Mullins(UCSF)(Belin et al., 2013). Full length K853A-mDia2 was generated based on the full-length WT-mDia2 (plasmid 54158, Addgene). Site directed mutagenesis was performed to generate the mutants, using QuikChange Lightning following manufacturer's instructions. The construct of GFP-myc-DAD(Alberts, 2001; Palazzo et al., 2001) was used as the template to make all DAD constructs in this study. NLS-flag-tagged actin(Posern et al., 2002) were kind gift from the Grosse Lab (University of Marburg) and was used as template to make the constructs used in this study. The shRNA against MgcRacGAP was MISSION shRNA plasmid DNA from Sigma (clone NM_013277.2-456s1c1). The siRNA oligos used in this study were the same as those described before(Liu and Mao, 2016), except siRNA against IPO9 (s31299, SilencerSelect siRNA from ThermoFisher). Primary antibodies used in this study include: rabbit anti mDia2 (Watanabe et al., 2008), mouse anti CENP-A (Ab13939, Abcam), mouse anti tubulin (T6199, Sigma), chicken anti GFP (Ab16901, Millipore), rabbit anti MgcRacGAP (Ab61192, Abcam), rabbit anti Flag (F7425, Sigma), rabbit anti IPO9 (Ab124710, Abcam), and rabbit anti H4K20me2 (Ab9052, Abcam).

Cell culture, transfection, and drug treatment

HeLa cells were used for most of the quantitative imaging experiments in this study. A HeLa cell line stably expressing YFP-CENP-A was used for high-resolution ratiometric live cell imaging. A HeLa cell line stably expressing EGFP-HJURP was also used for fixed cell imaging to examine HJURP turnover at centromeres. A U2OS cell line stably expressing Utr230-EGFP-NLS was used for longer term live imaging from mitotic exit to G1. All cells were maintained in DME medium supplemented with 10% FBS (complete growth medium) at 37°C in 5% CO2. The transfection of siRNAs was performed with Hiperfect (Qiagen) or DharmaFECT DUO (Dharmacon) following the manufacturers' protocols. For co-transfection experiments, siRNAs were transfected with at least 20-fold molar excess to marker plasmids encoding fluorescent proteins. Control cells were transfected with GAPDH siRNA. All knockdowns were confirmed by immunoblotting analysis. Cells were fixed for immunostaining or imaged 48 hours after transfection, or at time points specified in certain experiments. Thymidine synchronization was performed with 2 mM thymidine in complete growth medium for at least 17 hr, washed twice in pre-warmed PBS, and released into complete medium supplemented with 24 μM deoxycytidine (for 9 hr before entering mitosis). All chemicals used in the study were purchased form Sigma-Aldrich.

Visualizing nuclear actin short filaments with Utr230-EGFP-NLS probe in live G1 cells

Schematic procedure is summarized in **Figure 1A**. Briefly, HeLa cells were co-transfected with siRNA and mCherry vector (co-transfection marker) 48 hr prior to imaging, following aforementioned general transfection procedures. Upon releasing from the thymidine arrest (12 hr prior to imaging), cells were transfected with Utr230-EGFP-NLS using the DharmaFECT Duo transfection reagent following manufacturer's instructions. Live imaging was carried out using a

Olympus IX81 widefield microscope with a 60× NA 1.42 Plan Apochromat oil immersion objective (Olympus), a monochrome CCD camera (Sensicam QE; Cooke Corporation) at 1×1 binning, controlled by the SlideBook software (3i). Cells growing on poly-d-lysine–coated 35-mm glass-bottom dishes (MatTek Corporation) were maintained in CO2 independent medium (Gibco 18045) supplemented with 4 mM l-glutamine and 10% FBS, inside a chamber controlled at 37°C during imaging. Only single Z-section was imaged, and the movie was taken every 2 sec. An additional 1.6x optical magnifier was used to increase resolution. Cells containing both mCherry (indicator of siRNA transfection) and Utr230-EGFP-NLS were documented as short movies and categorized based on the patterns of spatiotemporal dynamics of the Utr230-EGFP-NLS probe. Three categories of distributions were observed: "nuclear punctate", "nuclear diffusive" and "cytoplasmic only". The "nuclear punctate" category distinguishes itself from the "nuclear diffusive" category with multiple small and motile particles inside the nucleoplasm (**Video S1**), which is not observed in "nuclear diffusive" category. The "cytoplasmic only" category has no discernable nuclear signals and only constitutes a small fraction of all the transfected cells. For longer-term live imaging of U2OS cells stably expressing Utr230-EGFP-NLS (FACS sorted for relatively low expression level), a Leica SP8 confocal microscope with the 40× HC PL Apo CS2 oil objective (NA 1.30) or 63× HC PL Apo CS2 oil objective (NA 1.40) and a temperature-controlled chamber was used. Cells were synchronized with double thymidine arrest and were kept in the same imaging media as above for live cell imaging. Image acquisition was done every 10 min with ≥ 9 Z-sections at intervals of 1 µm.

Quantitative fixed cell imaging and image analysis

Thymidine synchronization was used for all quantitative fixed cell imaging to allow for examination of centromeric CENP-A levels or concurrent events at about 2 hours after mitotic exit. Immunofluorescence and fixed cell imaging, as well as quantitative image processing using the INCA method were performed as previously described(Liu and Mao, 2016). Briefly, cells grown on poly-d-lysine–coated coverslips were washed in prewarmed PBS, fixed in cold MeOH at −20°C for 5 min, and then permeablized at room temperature with 0.1% Triton X-100 in PBS for 1 min. Cells were then washed briefly with PBS, and blocked in PBS containing 5% BSA at 4°C overnight. Coverslips were stained, at room temperature for 1 h, with primary antibodies diluted in PBS and then for another hour with Alexa Fluor 488–, DyLight 594–, or Cy^{TM}5-conjugated secondary antibodies. DAPI (16.67 ng/ml) was used for DNA staining. Coverslips were mounted using antifade reagent (ProLong Gold; Molecular Probes). Most image acquisition were performed at room temperature using an inverted microscope (IX81; Olympus) with a 60× NA 1.42 Plan Apochromat oil immersion objective (Olympus), a monochrome CCD camera (Sensicam QE; Cooke Corporation) at 1×1 binning, controlled by the SlideBook software (3i). Ten Z-sections spanning 5 µm at intervals of 0.5 µm were acquired for each field. To examine the localization of Utr230-EGFP-NLS in relation to centromeres, synchronized U2OS cells stably expressing Utr230-EGFP-NLS were fixed 2 hours after mitotic exit (11 hour after releasing from the 2nd thymidine arrest), using freshly prepared 3.7% PFA in PBS at room temperature for 15 min. Cells were then permeabilized with 0.1% Triton-X-100 in PBS at room temperature for 3 min, followed by blocking and antibody staining described above. Images were acquired on a DeltaVision Elite microscope (GE) with a 100x NA 1.4 oil immersion objective, as Z-stacks containing 25 sections at intervals of 0.2 µm. All images in each experiment and corresponding controls were acquired on the same day with identical exposure time. Enrichment

of Utr230-EGFP-NLS fluorescence intensity in the vicinity of centromeres were analyzed with MATLAB and ImageJ, using individual binary masks (slightly larger than each centromere) generated automatically based on ACA staining.

High resolution ratiometric live cell imaging and automated image analysis

Live cell imaging was performed as described previously (Liu and Mao, 2016) and above (using Olympus IX81 microscope). Quantitative analysis of centromereic YFP-CENP-A movies were conducted in MATLAB using custom code, with part of the measurement dependent on the mixed-model Gaussian fit in μ–track (Gaudenz Danuser Lab and Khuloud Jaqaman Lab, UTSW)(Jaqaman et al., 2008). Briefly, single centromeric focus of fluorescence were automatically detected and processed for intensity measurement as a reasonable estimate for YFP-CENP-A level at each centromere. All centromeric foci intensity was then normalized against the 'unloaded' frame's intensity and averaged for every time point in one single cell, in order to generate a time-lapse averaged intensity profile for each cell. Multiple cells' time-lapse intensity traces were finally pooled for statistical analysis.

Cell fractionation and immunoblotting analysis

Cell fractionation and immunoblotting analysis were performed as previously described(Liu and Mao, 2016), except that cellular fractionation only separated the cytoplasmic fraction and the nuclear pellet.

Live imaging of centromere movement, single-particle tracking and analysis

With the same wide-field microscopy setup as described before (Olympus IX81), HeLa cells stably expressing YFP-CENP-A were imaged from metaphase to early G1 every 5 min, across 11 z-sections 1 μm apart at every time point(Spagnol and Noel Dahl, 2014). Maximum z-projections were generated for each time point in the movie, based on which single-particle tracking and analysis was performed, using primarily the MATLAB based software μ–Track (Jaqaman et al., 2008). Only cells that survived at the end of movie and those without obvious nuclear rotation are included in our analysis. The frame at 25 min post anaphase onset, when most cells have their centromeres spread out well enough while largely remaining unloaded of CENP-A, was considered the beginning of each track. Approximately 36 frames spanning the 25 min to 200 min window were subjected to Gaussian mixture-model fitting to detect the coordinates of centromeres at sub-pixel resolution. Coordinates of centromeres at each frame were then subjected to drifting correction, following the equations below, for any given centromere at time point (i):

$$X_i' = X_i - \frac{\sum_1^N X_i}{N}$$

$$Y_i' = Y_i - \frac{\sum_1^N Y_i}{N}$$

Where N is the total number of centromeres at time point i, X_i and Y_i are raw coordinates per centromere at time point i, X_i' and Y_i' are updated coordinates corrected for global drifting. This way global long-range movement of the whole cell is eliminated so that only the motion inside the nucleus relative to the cell is reflected as a change of coordinates. Reverse tracking was performed using the adjusted coordinates with default parameters in μ–track. Trajectory analysis was performed upon the resultant tracks using μ–track(Ewers et al., 2005; Jaqaman et al., 2008) with tracks whose lengths are at least 20 frames, following the principles below:

$$\mu_{\nu,l}(\Delta n) = \frac{1}{M_l - \Delta n} \sum_{n=1}^{M_l-\Delta n} |x_l(n+\Delta n) - x_l(n)|^{\nu}$$

Where $x_l(n)$ is the position vector on trajectory l at time $n\Delta t$ for n = 1, 2, 3 …, M_l. M_l is the total number of positions in the trajectory l . Δt is the true time interval between frames. $\mu_{\nu,l}(\Delta n)$ is the moment of order ν for a given shift spanning n frames, consistent with a time shift $\delta t = \Delta n \Delta t$. Euclidean distance is denoted by |…|. In particular, the condition where ν = 2 is Mean Square Displacement (MSD). Because each moment is dependent on the time shift following a power law,

$$\mu_n(\delta t) \propto \delta t^{\gamma\nu}$$

The scaling coefficient was then computed with least-square linear regression of $\log(\mu_n)$ as a function of $\log(\delta t)$. A similar MSD analysis was also conducted(Tarantino et al., 2014) which led to the same conclusions (data not shown). Notably, in the ensemble MSD curve, only the first 25% of the curve were subjected to least-square linear fit(Saxton, 2007). Relative apparent diffusion coefficients were computed using μ–track, in arbitrary unit.

To quantify the change of intensity over time for each track, relative YFP-CENP-A loading ratio was defined as follows, in order to reflect the levels of CENP-A loading during an early time window of G1:

$$LR = \frac{\sum_{90\ min}^{140\ min} I(t)}{N \cdot Med}$$

Where *LR* is the YFP-CENP-A relative loading ratio, *I(t)* is the intensity at time point (t) post anaphase onset, *N* is the total number of frames with intensity information between 90 min and 140 min, '*Med*' is the median value of all tracks' intensity values within the first two frames (25min, 30min). The range 90-140 min was empirically chosen so that the maximum initial loading capacity is captured prior to inevitable fluorescent quench near the end of the movies. We understand that this algorithm may underestimate the actual loading ratio, yet nevertheless believe this is the best way to stringently reveal any differences in loading capacity in early G1. '*Med*' was determined to be a robust point estimate of common intensity of all tracks prior to most CENP-A loading (this estimate is necessary as not all tracks were detectable in the first two frames, making it otherwise impossible to compute the ratio).

Statistical analysis and plotting

All statistical analyses were performed with GraphPad Prism 5 (GraphPad) using unpaired, two tailed *t*-test between groups unless otherwise specified in figure legends (e.g. Mann-Whitney test and Fisher's exact test performed using GraphPad; Kolmogorov-Smirnov test performed with MATLAB; or z-test performed with MATLAB to compare two sample proportions). All plots were prepared in Prism (GraphPad) or MATLAB (MathWorks, R2018a). Control groups and specific experimental groups in all experiments were pooled together after normalization and presented.

SUPPLEMENTAL REFERENCES

Alberts, A.S. (2001). Identification of a Carboxyl-terminal Diaphanous-related Formin Homology Protein Autoregulatory Domain. Journal of Biological Chemistry *276*, 2824-2830.

Baarlink, C., Wang, H., and Grosse, R. (2013). Nuclear Actin Network Assembly by Formins Regulates the SRF Coactivator MAL. Science *340,* 864-867.

Belin, B.J., Cimini, B.A., Blackburn, E.H., and Mullins, R.D. (2013). Visualization of actin filaments and monomers in somatic cell nuclei. Molecular Biology of the Cell *24*, 982-994.

Ewers, H., Smith, A.E., Sbalzarini, I.F., Lilie, H., Koumoutsakos, P., and Helenius, A. (2005). Single-particle tracking of murine polyoma virus-like particles on live cells and artificial membranes. P Natl Acad Sci USA *102*, 15110-15115.

Jaqaman, K., Loerke, D., Mettlen, M., Kuwata, H., Grinstein, S., Schmid, S.L., and Danuser, G. (2008). Robust single-particle tracking in live-cell time-lapse sequences. Nat Meth *5*, 695-702.

Liu, C., and Mao, Y. (2016). Diaphanous formin mDia2 regulates CENP-A levels at centromeres. The Journal of Cell Biology *213*, 415-424.

Palazzo, A.F., Cook, T.A., Alberts, A.S., and Gundersen, G.G. (2001). mDia mediates Rho-regulated formation and orientation of stable microtubules. Nat Cell Biol *3*, 723-729.

Posern, G., Sotiropoulos, A., and Treisman, R. (2002). Mutant Actins Demonstrate a Role for Unpolymerized Actin in Control of Transcription by Serum Response Factor. Molecular Biology of the Cell *13*, 4167-4178.

Saxton, M.J. (2007). Modeling 2D and 3D Diffusion. In Methods in Membrane Lipids, A.M. Dopico, ed. (Totowa, NJ: Humana Press), pp. 295-321.

Spagnol, S.T., and Noel Dahl, K. (2014). Active cytoskeletal force and chromatin condensation independently modulate intranuclear network fluctuations. Integrative Biology *6*, 523-531.

Tarantino, N., Tinevez, J.-Y., Crowell, E.F., Boisson, B., Henriques, R., Mhlanga, M., Agou, F., Israël, A., and Laplantine, E. (2014). TNF and IL-1 exhibit distinct ubiquitin requirements for inducing NEMO–IKK supramolecular structures. The Journal of Cell Biology *204*, 231-245.